Journal of Cleaner Production 374 (2022) 134038

Contents lists available at ScienceDirect

Journal of Cleaner Production

journal homepage: www.elsevier.com/locate/jclepro

# Limits on the integration of power to gas with blast furnace ironmaking

Manuel Bailera [a,b,*], Takao Nakagaki [a], Ryoma Kataoka [a]

[a] Graduate School of Creative Science and Engineering, Waseda University, Okubo, Shinjuku-ku, Tokyo, 169-8555, Japan
[b] Escuela de Ingeniería y Arquitectura. Universidad de Zaragoza, Campus Río Ebro, María de Luna 3, 50018, Zaragoza, Spain

ARTICLE INFO

Handling editor: Panos Seferlis

*Keywords:*
Rist diagram
Power-to-Gas
Ironmaking
Methanation
Iron and steel
Synthetic natural gas

ABSTRACT

This article compares 16 Power to Gas integrations for blast furnace ironmaking by using 17 key performance indicators. The study includes 4 types of PtG ($PtH_2$, PtSNG using pure $CO_2$, PtSNG using treated BFG, and PtSNG using BFG), two types of blast furnaces (air-blown and oxygen) and two types of fossil replacement (coal or coke). The blast furnaces are modelled using the Rist diagram, validated with literature data (<2% deviation). For most cases, the decrease in total $CO_2$ emissions is around 150–215 $kg_{CO2}/t_{HM}$ per MW/($t_{HM}$/h) of electrolysis. The energy penalty (in terms of electricity consumption) was found to be mostly independent on the size of the PtG plant, but greatly dependent on the type of integration (10.1–20.6 MJ/$kg_{CO2}$). If significant $CO_2$ reductions are aimed, self-sufficiency in electricity consumption will not be achieved. In practice, the maximum PtG capacity to install is limited by the decrease in the flame temperature. In this context, the PtSNG integration consuming treated BFG, applied to OBF for coal replacement, provides the best results. Assuming a 500 $t_{HM}$/h blast furnace, the PtG capacity of this concept could be as large as 490 MW and avoid up to 21% of the $CO_2$ emissions.

## 1. Introduction

The ironmaking industry is one of the most energy- and carbon-intensive industries in the world. It is the second largest consumer of industrial energy (7,200 TWh/y) (Quader et al., 2015), and responsible of 9% of the total $CO_2$ emissions worldwide (International Energy Agency, 2020), accounting for (3.7 $Gt_{CO2}$/y) (De Ras et al., 2019). The main manufacturing route in ironmaking is blast furnaces (Fenton and Tuck, 2019). In blast furnaces, iron ore and coke are introduced at the top. The former is reduced while descending by using a reducing gas that ascends in counter-current. The reducing agents are CO (Eq. (1) to Eq. (3)) and $H_2$ (Eq. (4) to Eq. (6)) (Babich et al., 2008). This gas is produced at the lower part of the furnace by burning the coke with $O_2$-enriched air that is injected through the tuyeres (air separation unit needed). Auxiliary fuels, such as pulverized coal or natural gas can be also injected through the tuyeres to decrease the coke input (Fig. 1) (Geerdes et al., 2020).

$$3Fe_2O_3 + CO \rightarrow 2Fe_3O_4 + CO_2 \quad (1)$$

$$Fe_3O_4 + CO \rightarrow 3FeO + CO_2 \quad (2)$$

$$FeO + CO \rightarrow Fe + CO_2 \quad (3)$$

$$3Fe_2O_3 + H_2 \rightarrow 2Fe_3O_4 + H_2O \quad (4)$$

$$Fe_3O_4 + H_2 \rightarrow 3FeO + H_2O \quad (5)$$

$$FeO + H_2 \rightarrow Fe + H_2O \quad (6)$$

Because of the requirement of high-temperature heat (above 800–1,200 °C) and the nature of the process itself ($CO_2$ release during reduction), the blast furnace ironmaking process cannot be decarbonized with electrification (Ueckerdt et al., 2021). Renewable hydrogen and synthetic fuels can overcome this barriers (Ueckerdt et al., 2021). Within this framework, some authors have studied the application of Power to Gas (PtG) to blast furnace ironmaking. Power to Gas technology consumes renewable electricity to produce $H_2$, which is then combined with the $CO_2$ emissions of the ironmaking process to obtain synthetic methane (Bargiacchi et al., 2021). This synthetic fuel is used in the blast furnace to keep carbon in a closed loop (Perpiñán et al. (2021)), thus avoiding geological storage (the transport and storage costs represent the 30% of the overall costs in the CCS chain (Holz et al., 2018)). The studies found in literature show that the $CO_2$ emissions could be cut by 13%–19% (Hisashige et al., 2019), by using electrolysis power capacities of about 880 MW (Rosenfeld et al., 2020). Additionally, Bailera et al. (2021a) proposed the combination of Power to

* Corresponding author. Graduate School of Creative Science and Engineering, Waseda University, Okubo, Shinjuku-ku, Tokyo, 169-8555, Japan.
*E-mail address:* mbailera@unizar.es (M. Bailera).

https://doi.org/10.1016/j.jclepro.2022.134038
Received 18 April 2022; Received in revised form 11 August 2022; Accepted 4 September 2022
Available online 9 September 2022

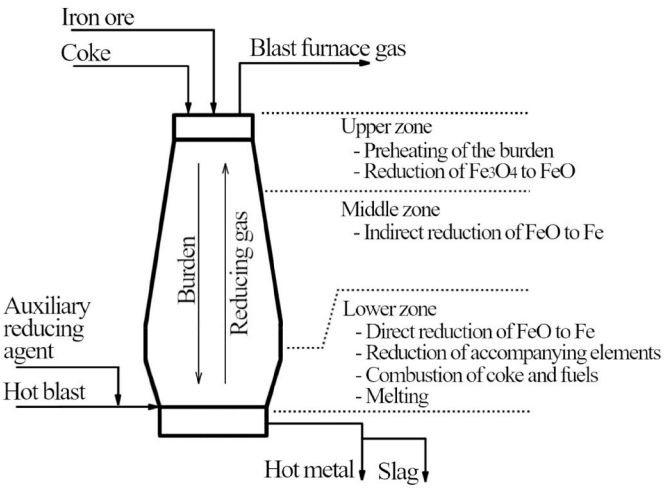


**Fig. 1.** Conceptual diagram of a blast furnace.

Methane with oxygen blast furnaces (OBF). In oxygen blast furnaces, pure oxygen is used for combustion instead of air, thus obtaining a top gas with very little contain of nitrogen. Since the water electrolysis of the PtG by-produces $O_2$, it allows diminishing the electricity consumption of the air separation unit that feeds the oxygen blast furnace. A first approach to this OBF-PtG system was studied by Perpiñán et al., 2021 by using overall energy and mass balances. Assuming 430 MW electrolysis power capacity, he found $CO_2$ emissions reduction of 8% and specific electricity consumptions of 34 MJ/$kg_{CO2}$.

In order to clearly establish the potential of Power to Gas within the ironmaking industry, the present paper analyzes 16 different PtG integrations and compares them with each other by using 17 key performance indicators. The results are provided as a function of the PtG capacity installed per $t_{HM}$/h produced in the blast furnace, in order to make them scalable to any size of PtG and ironmaking plants. Thus, this study provides several major novelties: (i) most of the 16 PtG integrations have not been assessed before in literature, (ii) all the integrations are assessed under the same framework for proper comparison, (iii) 17 key performance indicators are defined as a useful tool for standard comparison in further studies, (iv) the limits on the integration of PtG with blast furnace ironmaking are defined according to technical criteria, (v) recommendations on the best PtG configurations are provided, comparing $PtH_2$ with PtSNG. The paper is divided in the following sections: first, the case studies are defined (Section 2); then, the methodology is explained (Section 3); third, the results are presented and discussed, including the validation of the model, the individual analysis of each KPI, and the overall comparison (Section 4); finally, conclusions are provided (Section 5). The paper also includes an exhaustive appendix with graphs of all the KPIs (see supplementary material).

## 2. Potential integrations of power to gas with blast furnaces

When it comes to Power to Gas integrations, we can follow a decarbonization approach based on $PtH_2$ or PtSNG. The former is a straighter pathway that directly injects the renewable $H_2$ in the blast furnace to replace some fossil fuel. In the latter, the $H_2$ is combined with the $CO_2$ emitted by the ironmaking process to produce synthetic natural gas for injection, what keeps carbon in closed loop. Depending on the $CO_2$ source used in this methanation process (captured $CO_2$, treated BFG or BFG itself), three process flow diagrams for the PtSNG route can be established (Fig. 2). Therefore, we have 4 types of Power to Gas integrations. These are assessed for air-blown blast furnaces and for oxygen blast furnace. In addition, it is considered the possibility of replacing either coal or coke when injecting the renewable gas (when replacing

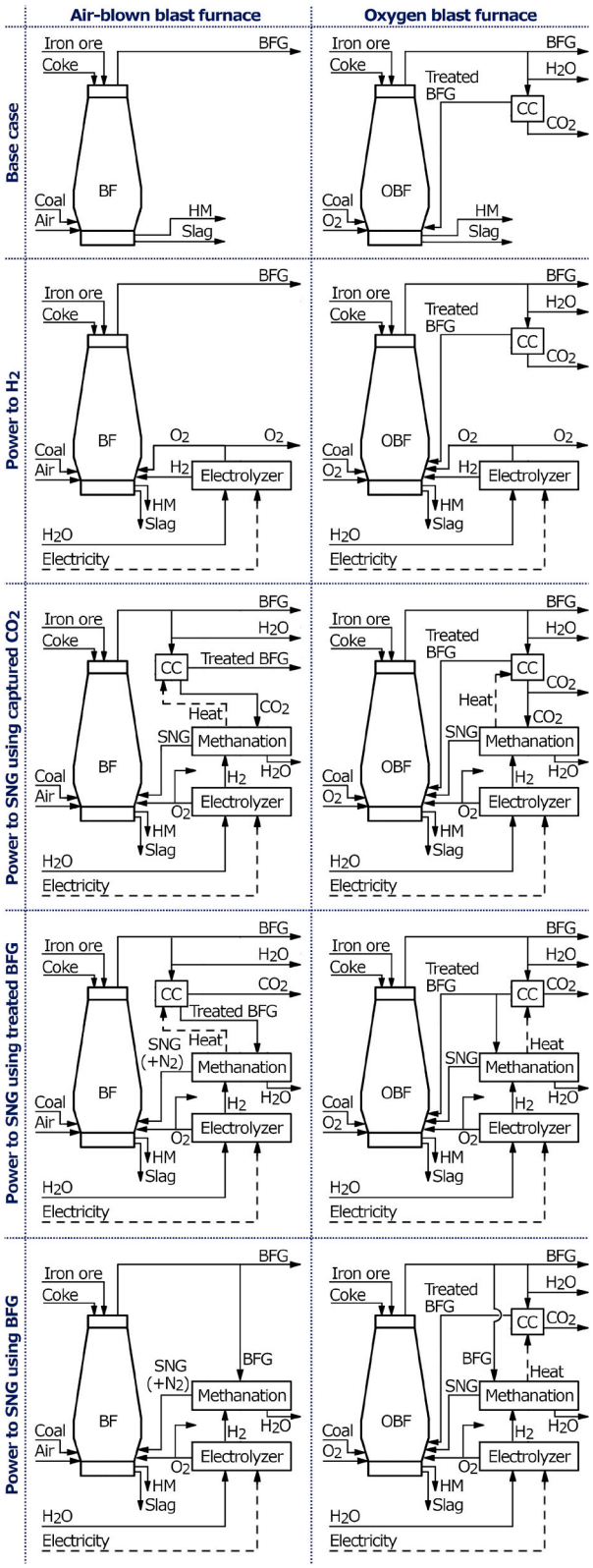


**Fig. 2.** Potential integrations of Power to Gas with blast furnace.

coke, the coal flow keeps unchanged, and vice versa). Thus, we have 16 study cases in total (4 types of PtG integration × 2 types of blast furnace × 2 types of fossil replacement), which are compared with each other and with their corresponding base case (where no integration is included).

It is worth to highlight that OBF configurations have in general three

main advantages with respect to BF configurations. The first one is the availability of a carbon capture process already in the base case scenario. Oxygen blast furnace are usually operated with top gas recycling (Shao et al., 2021), which rejects $CO_2$ from the BFG to inject the resulting mixture into the blast furnace as reducing agent and heat sink. Therefore, we can take advantage of this existing carbon capture stage when integrating the methanation process (in conventional BF, the carbon capture has to be installed on purpose). The second advantage comes from the greater amount of pure $O_2$ used in OBF (>70% $O_2$-enriched air). When installing large Power to Gas capacities (aiming for relevant decarbonization), most of the available $O_2$ from the electrolyzer will remain unused in BF configurations (since it is not needed), what reduces the impact of the integration. Oxygen blast furnaces can take advantage of all the $O_2$ available from the electrolysis stage. The third advantage arise when using treated BFG or BFG itself in the methanation process. In the case of air-blown blast furnaces, the large amount of $N_2$ present in the BFG (~50 vol%) will end up entering into the methanation stage and forming part of the final SNG (see supplementary material). This drastically reduces the fossil fuel replacement ratio (part of the SNG is just inert $N_2$) and decreases the flame temperature in excess ($N_2$ acts as sink of heat). When using OBF, the $N_2$ content in the BFG is around 1–2%, thus avoiding these issues.

## 3. Methods

### 3.1. Modelling methodology

#### 3.1.1. Blast furnace

The blast furnace is modelled using the Rist diagram (Fig. 3) (Rist and Meysson, 1967). This methodology allows for predicting variations in blast furnaces' performance when their operating conditions are changed. It uses the carbon, oxygen, hydrogen and energy balances, which are graphically depicted using the operation line. The methodology was thoroughly described in a previous paper by the authors (Bailera et al., 2021b), therefore only a short description is presented here. The equation of the operating line is written as Eq. (7). The slope, μ, stands for the number of moles of reducing gas needed for the production of 1 mol of Fe. The intercept, $Y_E$, gives the moles of $H_2$ and O coming from sources other than iron oxides that contribute to the formation of the reducing gas (Meysson et al., 1964).

$$Y = \mu \cdot X + Y_E \tag{7}$$

In practice, the operating line cannot be directly computed by calculating μ and $Y_E$ because data is missing. The operating line must be computed using two characteristic points denoted as R and P. The point R is given by the equilibrium between gas and solids in the mid zone of the blast furnace, and the point P is given by the energy balance of the system. Relevant results can be obtained from the operating line once characterized. Its slope stands for the required reducing agent rate in terms of C and $H_2$ per mole of Fe, so the coke input can be calculated (Hisashige et al., 2019). The intercept is the sum of the hydrogen and oxygen brought into the furnace (except for the $O_2$ contained in the iron ore). Therefore, by subtracting all other $O_2$ and $H_2$ sources (moisture, auxiliary fuels, coke and impurities), the necessary air flow rate can be derived (Hisashige et al., 2019). Additionally, the calculated rates of reducing agent and oxygen will determine the flame temperature. Also, the initial oxidation state of the iron oxides introduced in the blast furnace ($Y_A$) allows to derive the final degree of oxidation of the gas leaving the top of the furnace ($X_A - 1$). Finally, the ratio between direct and indirect reduction is identified by construction. The abscissa X = 1 gives the oxygen removed by direct reduction, $y_d$ (Fig. 3), and thus the oxygen removed by indirect reduction is easily calculated as $y_i = Y_A - y_d$.

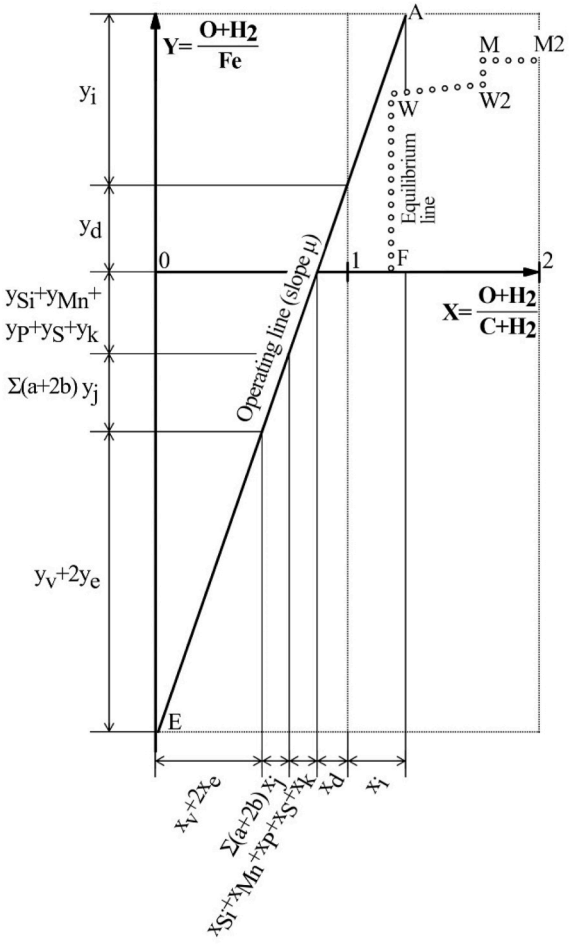


**Fig. 3.** Rist diagram.

#### 3.1.2. Power to gas, carbon capture plant and air separation unit

The process flow diagram of the Power to Gas plant is depicted in Fig. 4. It comprises an electrolyser (4.5 kWh/$Nm^3$ (Davies et al., 2021)) and two isothermal methanation reactors (370 °C and 320 °C, both at 5 bar) with water condensation after each stage (at 35 °C). This configuration allows reaching methane contents above 95 vol% (Izumiya and Shimada, 2021) (see supplementary material for SNG composition).

The amount and composition of the final SNG is calculated by chemical equilibrium of the methanation reaction (Bailera et al., 2019). The methanation of $CO_2$ (Eq. (8)) can be decomposed as the combination of the reverse water-gas shift reaction (Eq. (9)) and a subsequent CO methanation (Eq. (10)) (Gao et al., 2012).

$$CO_2 + 4H_2 \leftrightarrow CH_4 + 2H_2O \tag{8}$$

$$CO_2 + H_2 \leftrightarrow CO + H_2O \tag{9}$$

$$CO + 3H_2 \leftrightarrow CH_4 + H_2O \tag{10}$$

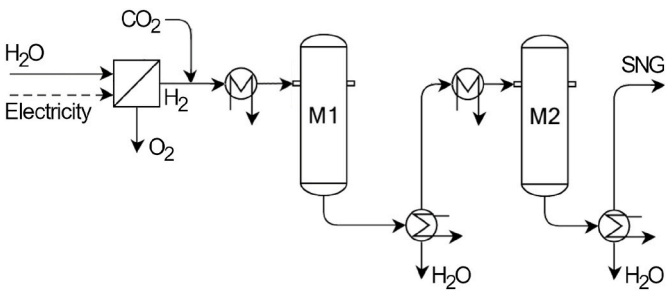


**Fig. 4.** Process flow diagram of the Power to SNG plant.

The products of the $CO_2$ methanation are calculated through the mole balance of the overall reaction (Eq. (11)),

$$\nu_{CO2}CO_2 + \nu_{H2}H_2 + \nu_{CH4}CH_4 + \nu_{H2O}H_2O + \nu_{CO}CO \leftrightarrow \mu_{CO2}CO_2 + \mu_{H2}H_2 + \mu_{CH4}CH_4 + \mu_{H2O}H_2O + \mu_{CO}CO \quad (11)$$

where $\nu_i$ are the initial moles of reagent $i$, and $\mu_i$ the final moles of product $i$. The latter are the five unknown variables that give the gas composition after the reaction. These are computed through the mole balances of carbon, hydrogen and oxygen (Eq. (12) to Eq. (14)) and through the equilibrium constants of the involved reactions (Eq. (15) and Eq. (16)).

$$\nu_{CO2} + \nu_{CH4} + \nu_{CO} = \mu_{CO2} + \mu_{CH4} + \mu_{CO} \quad (12)$$

$$\nu_{H2} + 2\nu_{CH4} + \nu_{H2O} = \mu_{H2} + 2\mu_{CH4} + \mu_{H2O} \quad (13)$$

$$\nu_{CO2} + \frac{1}{2}\nu_{H2O} + \frac{1}{2}\nu_{CO} = \mu_{CO2} + \frac{1}{2}\mu_{H2O} + \frac{1}{2}\mu_{CO} \quad (14)$$

$$Kp_{RWGS} = \frac{\mu_{CO}\mu_{H2O}}{\mu_{CO2}\mu_{H2}} \quad (15)$$

$$Kp_{CO} = \frac{\mu_{CH4}\mu_{H2O}(\mu_{CO2} + \mu_{H2} + \mu_{CH4} + \mu_{H2O} + \mu_{CO})^2}{\mu_{H2}^3\mu_{CO}}\left(\frac{P_r}{P_a}\right)^{-2} \quad (16)$$

$Kp_i$ is the equilibrium constant of reaction $i$, $P_r$ is the pressure inside the reactor, and $P_a$ is the ambient pressure. The value of $Kp_i$ is directly computed from its definition (Eq. (17)):

$$Kp_i = e^{-\frac{G_i}{R \cdot T_r}} \quad (17)$$

where $G_i$ is the Gibbs free energy of reaction $i$ (Eq. (18) and Eq. (19)), and $T_r$ the temperature of the reactor. It should be noted that the Gibbs free energy of each component can be computed as $g_i = h_i - T_r \cdot s_i$.

$$G_{RWGS} = g_{CO} + g_{H2O} - g_{H2} - g_{CO2} \quad (18)$$

$$G_{CO} = g_{CH4} + g_{H2O} - 3g_{H2} - g_{CO} \quad (19)$$

Regarding the carbon capture plant, amine scrubbing technology is chosen for the study. The amine plant is assumed to have 95% $CO_2$ capture efficiency (Kamijo et al., 2021) and 2.95 MJ/$kg_{CO2}$ specific consumption (Bailera et al., 2020). Lastly, the consumption of the air separation unit is set at 170 kWh/$t_{O2}$ (Lisbona et al., 2020).

### 3.2. Definition of the key performance indicators

The key performance indicators (KPI) quantify the most significant aspects that may have an impact on the overall system performance (Table 1). We use KPIs to establish the integration limits of Power to Gas in ironmaking. The three more restrictive KPIs will be $KPI_{01}$ (electrolysis electricity consumption), $KPI_{09}$ (flame temperature) and $KPI_{17}$ (thermal self-sufficiency). The first one will define the required power capacity of the electrolyzer, which should be in compliance with the state-of-the-art of the technology. Largest electrolysis projects are usually around 100 MW (Davies et al., 2021), while the most ambitious planned project aims to reach 600 MW (Thema et al., 2019). The second most restrictive KPI is the flame temperature reached when SNG or $H_2$ are injected into the blast furnace. According to literature, this temperature should not fall below 2,000 °C (Geerdes et al., 2020). The last KPI that may impose a limitation in PtG integration determines if the internal thermal consumptions of the steel plant are properly covered with the available BFG and COG. If not, additional fuel consumption should be needed, which is what we try to avoid. We do not consider electricity self-sufficiency as a limitation, since renewable electricity from solar or wind power could be used without increasing $CO_2$ emissions. In fact, it is expected to not reach electricity self-sufficiency due to the great consumption of the electrolyzer. Nevertheless, if some configurations meet both thermal and electrical self-sufficiency, they will be prioritized. Some of the KPIs are directly obtained as a result from the modelling methodology, while others need further explanation. The latter comprises $CO_2$ emissions, energy penalty and self-sufficiency, and they are detailed in the following subsections.

**Table 1**
Key performance indicators of Power to Gas integrations in ironmaking.

| KPI | Description | Units |
|---|---|---|
| $KPI_{01}$ | Electrolysis electricity consumption | MJ/$t_{HM}$ |
| $KPI_{02}$ | Mass flow of SNG or $H_2$ injected to the blast furnace | kg/$t_{HM}$ |
| $KPI_{03}$ | Substituted fossil fuel ratio | $kg_{coal}/kg_{SNG}$ or $kg_{coal}/kg_{H2}$ |
| $KPI_{04}$ | $O_2$ produced in the ASU | kg/$t_{HM}$ |
| $KPI_{05}$ | CO utilization, $\eta_{CO}$ | – |
| $KPI_{06}$ | $H_2$ utilization, $\eta_{H2}$ | – |
| $KPI_{07}$ | Percentage of direct reduction in the blast furnace | % |
| $KPI_{08}$ | Recirculation ratio in OBF concepts | % |
| $KPI_{09}$ | Flame temperature | °C |
| $KPI_{10}$ | Total $CO_2$ emissions | kg/$t_{HM}$ |
| $KPI_{11}$ | $CO_2$ emissions that can be stored in geological storage (emitted as pure $CO_2$) | kg/$t_{HM}$ |
| $KPI_{12}$ | Total avoided $CO_2$ | kg/$t_{HM}$ |
| $KPI_{13}$ | Avoided $CO_2$ that is kept in closed loop | kg/$t_{HM}$ |
| $KPI_{14}$ | Gross energy penalty of avoiding $CO_2$ | MJ/$kg_{CO2}$ |
| $KPI_{15}$ | Net energy penalty of avoiding $CO_2$ | MJ/$kg_{CO2}$ |
| $KPI_{16}$ | Electricity self-sufficiency | MJ/$t_{HM}$ |
| $KPI_{17}$ | Thermal self-sufficiency | MJ/$t_{HM}$ |

#### 3.2.1. $CO_2$ emissions

The BFG that is produced in the blast furnace may follow different processes. One part is recycled to the blast furnace as SNG (after methanation) and/or as treated BFG (after carbon capture). The rest may leave the system as BFG itself, as pure $CO_2$ or even as treated BFG (see Fig. 2). We define the total $CO_2$ emitted by the blast furnace ($KPI_{10}$) as the sum of the emissions of these three gases leaving the system. To quantify this, we compute the equivalent $CO_2$ emissions by taking into account that their CO content will end up as $CO_2$ after using the gases in other processes of the steel plant (1 mol of $CO_2$ gives 1 mol of $CO_2$, and 1 mol of CO will give 1 mol of $CO_2$ after combustion). In addition, we calculate the percentage of the total emitted $CO_2$ that can be directly sent to geological storage (i.e., the share that is emitted as pure $CO_2$, $KPI_{11}$).

To evaluate the effectiveness of the Power to Gas integrations, we also compute the avoided $CO_2$ ($KPI_{12}$), which is the difference between the total $CO_2$ emitted by a given configuration and its base case scenario. The $CO_2$ is avoided because part of the carbon is continuously recycled by using the methanation process, but also because the coal and coke replacement ratio is greater than 1 for the injected SNG (or $H_2$). The $CO_2$ that is kept in closed loop by going through methanation ($KPI_{13}$) is quantified to assess its contribution to the total $CO_2$ avoidance.

#### 3.2.2. Energy penalty

The gross energy penalty of avoiding $CO_2$ ($KPI_{14}$) is calculated as the quotient between the energy consumed (on account of Power to Gas) and the avoided $CO_2$ (Eq. (20)). The energy consumption includes the electricity supplied to the electrolyzer ($KPI_{01}$), the heat provided to the amine scrubbing for capturing the $CO_2$ used in methanation ($Q_{a,m}$), and the heat used to preheat the SNG (or $H_2$) that is injected in the blast furnace ($Q_{p,m}$). For consistency, the latter two are computed as the equivalent electricity that would be produced in the power plant with an efficiency $\eta_{pp} = 0.36$ (Kim and Lee, 2018).

$$KPI_{14} = \frac{KPI_{01} + (Q_{a,m} + Q_{p,m})\eta_{pp}}{KPI_{12}} \quad (20)$$

Since the Power to Gas integrations allow to save energy in other

processes of the plant, we can calculate a net energy penalty for the $CO_2$ avoidance ($KPI_{15}$). This follows Eq. (21), which accounts for the electricity that is no longer consumed in the air separation unit ($W_{ASU,m}$; assuming a typical specific consumption of 0.61 MJ/$kg_{O2}$ (Lisbona et al., 2020)), for the energy content of the substituted fossil fuel ($KPI_{02}KPI_{03}LHV_k$), and for the thermal energy available from the methanation process ($Q_{ex,m}$). For consistency, the latter two are computed as the equivalent electricity that would be produced in the power plant.

$$KPI_{15} = \frac{KPI_{01} - W_{ASU,m} + \left(Q_{a,m} + Q_{p,m} - KPI_{02}KPI_{03}LHV_k - Q_{ex,m}\right)\eta_{pp}}{KPI_{12}} \quad (21)$$

As first approach, $KPI_{14}$ and $KPI_{15}$ assume that all heats can be used in the power plant, independently of the temperature of the streams. To obtain more accurate values, a detailed integration of the streams should be performed within the entire process flow diagram of a steel plant. Nevertheless, as long as we established the same comparison framework for all the Power to Gas integrations, the comparison will be valid, which is the objective of this study. Moreover, the variation in the terms $Q_{a,m}$, $Q_{p,m}$ and $Q_{ex,m}$ will be mostly negligible when compared to $KPI_{01}$ (electrolysis electricity consumption), which is by far the largest consumption. Therefore, the change in the KPIs will be minor.

### 3.2.3. Self-sufficiency

The electricity consumption in steel plants is usually in the range 800–1,700 MJ/$t_{HM}$ (Perpiñán et al., 2021). This is supplied by burning COG and BFG in a power plant using a gas-fired boiler (24%–44% efficiency) or a gas turbine (46% efficiency) (Rainer Remus and Serge Roudier, 2013). The amount of COG produced in steel plants is in the range 110–160 kg/$t_{HM}$ (Bailera et al., 2021a), from which between the 10% and 75% is usually required for internal processes, leaving the rest available for power production in the power plant (Wu et al., 2016). Regarding the BFG, conventional air-blown blast furnaces with pulverized coal injection produce 1,900 to 2,300 kg/$t_{HM}$ (Bailera et al., 2021b), from which the 54%–58% is needed in internal processes (Suzuki et al., 2015), being the rest available for the power plant (Rainer Remus and Serge Roudier, 2013). Normally, there is an excess of thermal energy available for the power plant, so either the surplus electricity is sold to the grid or part of the gases is flared or sold to an external power plant. A summary of the range of values for these energy flows is depicted in Fig. 5a, assuming typical LHV for COG (41.6 MJ/kg) (Bailera et al., 2021a) and BFG (2.5 MJ/kg) (Bailera et al., 2021b).

In this study, we assume the base case scenario presented in Fig. 5b, which is around the mid value of the typical ranges found in literature for steel plants. The electricity consumption is 1,200 MJ/$t_{HM}$ and the thermal consumption covered with COG and BFG is 4,742 MJ/$t_{HM}$. The mass flows of COG and BFG produced in the steel plant are 140 kg/$t_{HM}$ and 1,967 kg/$t_{HM}$, which represent a total of 10,741 MJ/$t_{HM}$ of thermal energy available. The 44% of this energy is used to be self-sufficient in thermal energy consumption, the 31% is send to the power plant to be self-sufficient in electricity consumption (36% efficiency), and the remaining 25% would be available for selling or for additional processes. Our base case scenario is in line with data from a real steel plant of ArcelorMittal located in Gijón, Spain (570 $t_{HM}$/h in size) (ArcelorMittal, n.d., n.d.). In 2019, they planned to sell unused gases to a nearby power plant. This power plant, which would run only on steel gases, would produce 181 MW of electricity (Pandiello, 2019) with 34.5% efficiency (Robles et al., 2014). This means that the steel plant of ArcerlorMittal aimed to sell about 3,300 MJ/$t_{HM}$ of thermal energy in the form of excess steel gases. In our base case scenario, we have available 2,666 MJ/$t_{HM}$ as excess gases, so the proposed scenario is considered realistic.

Under PtSNG integrations, and specially for oxygen blast furnaces, the available BFG decreases (some part is used in methanation and other part in top gas recycling). Despite of this, we should keep constant the internal consumption of thermal energy (4,742 MJ/$t_{HM}$), so the percentage of BFG available for the power plant and selling will be lower. Eventually, the use of BFG in methanation, and the electricity consumption in the electrolyzer (which is added to the 1,200 MJ/$t_{HM}$

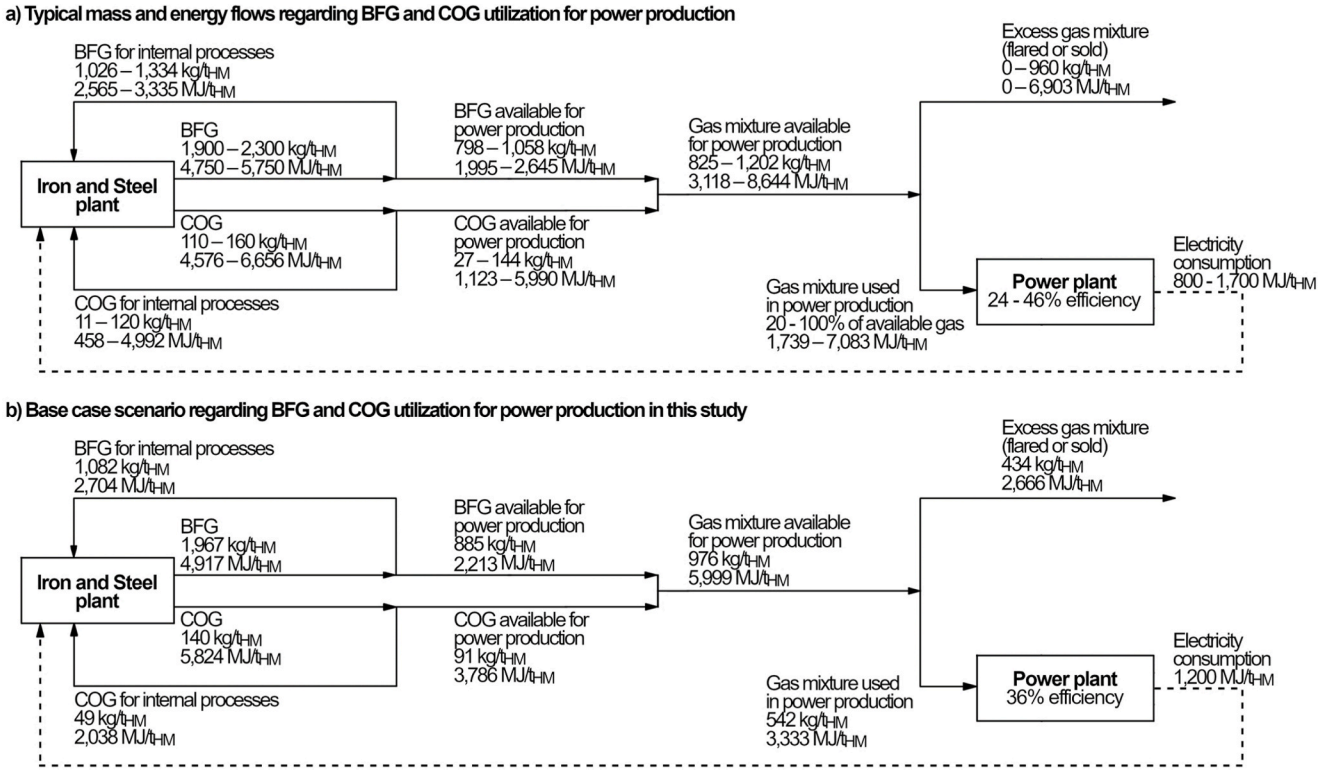


**Fig. 5.** Mass and energy flows regarding BFG and COG utilization in power production for self-sufficiency in steel plants.

baseline) will increase to the extent that there will be no excess gas for selling, and the power plant will not produce enough electricity. At this point, the steel plant is no longer self-sufficient, and electricity should be purchased from the grid to satisfy demand. The electricity purchased from the grid is assumed to come from renewable energy sources, in order to not increase the $CO_2$ emissions.

To quantify the electricity that can be sold or must be purchased we use the $KPI_{16}$ (Eq. (22)), which provides the electricity balance. It is a balance between the electricity that can be produced in the ironmaking plant with the available gases ($(5,824 + m_{BFG}LHV_{BFG} - 4,742 - Q_{p,m} - Q_{a,m} + Q_{ex,m})\eta_{pp}$), and the electricity that is consumed ($-\ 1,200 - KPI_{01} + W_{ASU,m}$). When $KPI_{16} > 0$, the steel plant is self-sufficient and $KPI_{16}$ represents the amount of electricity than can be sold to the grid, while when $KPI_{16} < 0$ the steel plant is not self-sufficient and $|KPI_{16}|$ is the amount of electricity that must be purchased from the grid. It takes into account the electricity consumption of the electrolyzer ($KPI_{01}$), the thermal energy required for preheating the injected SNG or $H_2$ ($Q_{p,m}$), the heat needed for amine scrubbing ($Q_{a,m}$), the heat available from methanation ($Q_{ex,m}$), and the electricity saved in the ASU thanks to the $O_2$ available from the electrolyzer ($W_{ASU,m}$).

data (Table 2), so it is considered to be validated.

To have a fair comparison, the base case of the oxygen blast furnace is elaborated taking the air-blown blast furnace as reference. The iron ore and coal inputs are the same, but the $O_2$-enrichment is increased to 99.5%. Also, 450 kg/$t_{HM}$ of treated top gas are recirculated at 900 °C (Jin et al., 2016) to keep the same flame temperature. The chemical efficiency remains unchanged, but the temperature of the chemical reverse zone (900 °C (Sato et al., 2015)), the heat evacuated by the staves (500 MJ/$t_{HM}$ (Sahu et al., 2015)) and the temperature of the BFG (85 °C (Babich et al., 2019)) are adjusted according to literature to have a consistent OBF operation. Thus, we obtain CO and $H_2$ utilization ratios of 45% and 24%, and a percentage of direct reduction of 16%, which are in agreement with literature (Sahu et al., 2015). The equivalent $CO_2$ emissions in this case are 1,163 kg/tHM, of which 42% are available as pure $CO_2$ from the amine carbon capture plant.

### 4.2. Key performance indicators

In this study we compare 16 case studies using 17 KPIs. All the KPIs are analyzed as a function of $KPI_{01}$, which is the electricity consumption of the electrolysis (i.e., as a function of the size of the Power to Gas plant). The results are summarized in this section, providing graphical representation only for the most relevant information. The rest of the graphs are available in the appendix for further clarification (see supplementary material). Moreover, relevant data are gathered in Table 3.

$$KPI_{16} = (5,824 + m_{BFG}LHV_{BFG} - 4,742 - Q_{p,m} - Q_{a,m} + Q_{ex,m})\eta_{pp} - 1,200 - KPI_{01} + W_{ASU,m} \quad (22)$$

Furthermore, if the sum within parenthesis in Eq. (22) becomes less than 0, then the steel plant would not have enough BFG and COG to satisfy its own thermal demands. This parenthesis is the available thermal energy for the production of electricity; if it becomes negative, it means that the thermal requirements are not fulfilled within the ironmaking plant, what would imply the purchase of "Heat" (i.e., increasing the fossil fuel consumption). This is denoted by $KPI_{17}$ (Eq. (23)). The requirement of $KPI_{17} > 0$ is considered as an integration limit for the electrolysis capacity that can be installed.

$$KPI_{17} = (5,824 + m_{BFG}LHV_{BFG} - 4,742 - Q_{p,m} - Q_{a,m} + Q_{ex,m}) \quad (23)$$

It should be noted that the term $m_{BFG}LHV_{BFG}$ stands for the energy content of the blast furnace gas that remains available after Power to Gas integration (in the case of BF-PtSNG-$CO_2$ integration, the energy of the treated BFG that is available should be also accounted). As occurred for the energy penalty, here we provide a common framework for comparison that allows identifying the best Power to Gas integration based on typical operating data of steel plants. To obtain more accurate results, calculations should be performed on a case-by-case basis, since the amount of COG available for power production, as well as the electricity consumption, vary depending on the steel plant.

## 4. Results and discussion

### 4.1. Validation of base case scenario

The base case of the air-blown blast furnace is based on data from Babich et al. (2019). This is a conventional blast furnace with pulverized coal injection and 26% $O_2$-enriched hot blast. The chemical efficiency is 92%, the temperature of the chemical reserve zone is 800 °C and the heat evacuated by the staves is 700 MJ/$t_{HM}$ (20% of this heat is evacuated in the upper zone) (Bailera et al., 2021b). As a result, we obtain that the CO and $H_2$ utilization ratios are 51% and 31%, the percentage of direct reduction is 30.6%, and the flame temperature is 2,138 °C. The equivalent $CO_2$ emissions of the blast furnace are 1,338 kg/$t_{HM}$. The model provides a discrepancy below 2% with respect to the reference

#### 4.2.1. $KPI_{02}$: mass flow of SNG or $H_2$ injected to the blast furnace

The gas production when using $PtH_2$ is 20 kg/h per MW of electrolysis, independently of the case study, which corresponds to the selected specific consumption of 4.5 kWh/$Nm^3$ (66.7% LHV efficiency). Similarly, the SNG production when using pure $CO_2$ is independent of the case study, obtaining 41 kg/h per MW of electrolysis. This corresponds to an electricity-to-chemical efficiency of 54%, typical of PtG concepts. In the case of using BFG in the methanation plant (treated or as is), the SNG production varies because the BFG composition depends on the case study (154–230 kg/h for BF, and 52.5–64.2 kg/h for OBF, per MW of electrolysis). In the BF cases, the mass flow of SNG produced is much greater but the major part is actually inert $N_2$ (it entered the methanation as part of the BFG). Besides, the higher the CO content in the BFG, the more SNG will be obtained (1 mol of CO requires 3 mol of $H_2$, Eq. (10), while 1 mol of $CO_2$ requires 4 mol of $H_2$, Eq. (8)). Since the LHV of the SNG obtained is 47.2–47.8 MJ/kg, and the LHV of the mixture of SNG + $N_2$ is 11.4–18.1 MJ/kg, the ratio between the energy content of the gas and the electricity consumed in the PtG is in the range 71%–84%. The higher value of 84% corresponds to the case of coal replacement in an OBF using treated BFG in the methanation plant. These energy ratios can be larger than the electrolysis efficiency itself because there is $H_2$ already existing in the BFG that enters into the methanation (treated BFG or as is).

#### 4.2.2. $KPI_{03}$: substituted fossil fuel ratio

The replacement ratios were found to be independent of the size of the Power to Gas plant. They mainly depend on the replaced fossil fuel (coal or coke) and on the gas used to replace it ($H_2$, SNG or SNG + $N_2$). When injecting SNG, the replacement ratio for coal is 1.30–1.40, and for coke is 1.10–1.15 (little difference between BF and OBF). The latter is in complete agreement with the value provided by Babich for the replacement of coke by methane, which is 1.13 (Babich, 2021). When

**Table 2**
Model results for base case scenarios.

| Inlet (kg/$t_{HM}$) | BF | | | OBF |
|---|---|---|---|---|
| | Babich (Babich et al., 2019) | Model | Δ (%) | Model |
| **Iron ore** | **1,558.0** | **1,558.0** | – | **1,558.0** |
| # $Fe_2O_3$ | 1,146.9 | 1,146.9 | – | 1,146.9 |
| # FeO | 187.3 | 187.3 | – | 187.3 |
| # $SiO_2$ | 69.9 | 69.9 | – | 69.9 |
| # $Al_2O_3$ | 107.2 | 107.2 | – | 107.2 |
| # CaO | 26.9 | 26.9 | – | 26.9 |
| # MgO | 16.2 | 16.2 | – | 16.2 |
| # MnO | 3.6 | 3.6 | – | 3.6 |
| T (°C) | 25 | 25 | – | 25 |
| **Coke** | **283.0** | **289.0** | **2.1** | **234.8** |
| #C | 251.4 | 256.7 | 2.1 | 208.6 |
| # $Fe_2O_3$ | 1.7 | 1.8 | 2.1 | 1.4 |
| # $SiO_2$ | 19.7 | 20.1 | 2.1 | 16.3 |
| # $Al_2O_3$ | 9.1 | 9.3 | 2.1 | 7.6 |
| # CaO | 0.8 | 0.8 | 2.1 | 0.6 |
| # MgO | 0.3 | 0.3 | 2.1 | 0.3 |
| T (°C) | 25 | 25 | – | 25 |
| **Coal** | **200.0** | **200.0** | – | **200.0** |
| #C | 153.6 | 153.6 | – | 153.6 |
| #H | 8.3 | 8.3 | – | 8.3 |
| #O | 10.2 | 10.2 | – | 10.2 |
| #N | 3.1 | 3.1 | – | 3.1 |
| #S | 0.9 | 0.9 | – | 0.9 |
| #$H_2O$ | 2.4 | 2.4 | – | 2.4 |
| # $SiO_2$ | 12.3 | 12.3 | – | 12.3 |
| # $Al_2O_3$ | 8.9 | 8.9 | – | 8.9 |
| # CaO | 0.3 | 0.3 | – | 0.3 |
| T (°C) | 25 | 25 | – | 25 |
| **Hot blast** | **1,172.1** | **1,181.7** | **0.8** | **333.4** |
| #$N_2$ | 826.7 | 833.5 | 0.8 | 1.5 |
| #$O_2$ | 345.4 | 348.2 | 0.8 | 331.9 |
| T (°C) | 1,200 | 1,200 | – | 1,200 |
| **Treated BFG** | – | – | – | **448.8** |
| #$N_2$ | – | – | – | 7.9 |
| # $CO_2$ | – | – | – | 25.7 |
| # CO | – | – | – | 407.3 |
| #$H_2$ | – | – | – | 8.0 |
| (°C) | – | – | – | 900 |
| **Outlet (kg/$t_{HM}$)** | | | | |
| **Hot metal** | **1,000.0** | **1,000.0** | **0.0** | **999.8** |
| # Fe | 947.2 | 947.2 | 0.0 | 947.0 |
| #C | 45.0 | 45.0 | 0.0 | 45.0 |
| # Si | 5.3 | 5.3 | 0.0 | 5.3 |
| # Mn | 2.5 | 2.5 | 0.0 | 2.5 |
| T (°C) | 1,500 | 1,500 | – | 1,500 |
| **Slag** | **260.0** | **261.8** | **0.7** | **256.0** |
| # $SiO_2$ | 90.4 | 91.0 | 0.7 | 87.2 |
| # $Al_2O_3$ | 124.6 | 125.4 | 0.7 | 123.7 |
| # CaO | 26.3 | 26.5 | 0.7 | 26.3 |
| # MgO | 16.4 | 16.5 | 0.7 | 16.4 |
| # MnO | 0.4 | 0.4 | 0.7 | 0.4 |
| # CaS | 1.9 | 1.9 | 0.7 | 1.9 |
| T (°C) | 1,550 | 1,550 | – | 1,550 |
| **BFG** | **1,953.2** | **1,966.9** | **0.7** | **1,519.2** |
| #$N_2$ | 830.0 | 836.6 | 0.8 | 12.5 |
| # $CO_2$ | 678.8 | 684.4 | 0.8 | 814.3 |
| # CO | 414.7 | 416.2 | 0.4 | 645.0 |
| #$H_2O$ | 23.9 | 23.8 | −0.6 | 34.8 |
| #$H_2$ | 5.9 | 5.9 | 0.0 | 12.6 |
| T (°C) | 150 | 150 | – | 85 |

injecting SNG + $N_2$, coal is replaced at a ratio 0.32–0.44, and coke at 0.29–0.37. Lastly, when injecting $H_2$ in the BF, the coal replacement is 2.90 and the coke replacement 2.46. These two values increase by 25% when the $H_2$ is injected in an OBF. It must be noted that when coke was replaced, coal was kept constant at 200 kg/$t_{HM}$ in the simulation (base case mass flow). Similarly, when coal was replaced, coke was kept constant at 289.0 and 234.8 kg/$t_{HM}$, for BF and OBF respectively (base case mass flows).

In general, the replacement ratios obtained for coal are 18% greater than those for coke, independently of the type of gas injected. This means that the replace of coke by coal is 0.85, which is in agreement with the correlation of Brower and Toxopeus (1991). This formula is based on real data from the Hoogovens IJmuiden blast furnace, and depends on the properties of the coal injected (see Appendix in supplementary material). It gives 0.87 coke replacement ratio for the coal we used (2% deviation between the model and the correlation).

#### 4.2.3. $KPI_{04}$: $O_2$ produced in the ASU

The rate at which the $O_2$ needs are cut is constant and similar for all SNG and SNG + $N_2$ injections. In these cases, the $O_2$ production in the ASU is decreased by 152–158 $kg_{O2}$/h per each MW of electrolysis, what actually equals the availability of the $O_2$ by-produced in the electrolyzer (159 $kg_{O2}$/h per MW). In the case of $H_2$ injections, the $O_2$ production in the ASU decreases even faster than this availability because the $O_2$ required in the blast furnace diminishes (we avoid the $O_2$ that was used to burn the C that no longer enters the blast furnace). Thus, the saving of $O_2$ in the ASU is 167 $kg_{O2}$/h for $H_2$ injections in BF and about 195 $kg_{O2}$/h for OBF, per each MW. The difference is greater in OBF because all the $O_2$ for the blast furnace is produced in the ASU. In air-blown BF, what is actually diminished is the air injection, what consequently decreases the $O_2$ required in the ASU because there is less air to enrich.

In the base case, the ASU produces 95.1 $kg_{O2}/t_{HM}$ for the BF, and 333.4 $kg_{O2}/t_{HM}$ for the OBF. At the mentioned saving rates, the ASU will no longer be need above 0.57–0.61 MW/($t_{HM}$/h) of electrolysis capacity for BF, and above 1.71–2.19 MW/($t_{HM}$/h) for OBF (the lower limit corresponds to $H_2$ injections and the upper to SNG).

#### 4.2.4. $KPI_{05}$ and $KPI_{06}$: CO and $H_2$ utilization

The operating line allows computing the overall gas utilization, $\eta_{CO,H_2}$, which is the quotient between the mole flow of $CO_2$+$H_2O$ and the mole flow of $CO_2$+$H_2O$ + CO + $H_2$ in the BFG. This gives an idea on how much reducing gas was used in the blast furnace. According to the Rist model, it decreases with the PtG capacity in most cases, although the variation is moderate (2.4 percentage points per $\frac{MW_{PtG}}{t_{HM}/h}$ as much) (see Fig. 6). Because of the larger content of CO and $CO_2$ compared to $H_2$ and $H_2O$, this parameter is mostly driven by the CO utilization.

To obtain separately the utilization of CO ($\eta_{CO}$) and $H_2$ ($\eta_{H_2}$), an additional energy balance on the upper zone of the blast furnace is performed (see (Bailera et al., 2021b)). The assumptions taken in this balance (constant heat removed by the staves and constant temperature of the BFG), influences the behavior of $\eta_{CO}$ and $\eta_{H_2}$, which is shown in the appendix (see supplementary material). In summary, the larger the PtG capacity, the greater the heat available in the upper zone of the blast furnace. Therefore, the $H_2$ utilization (endothermic process) increases in order to balance this heat (what subsequently diminish the CO utilization). The three main reasons for which there is more thermal energy available are: (i) the increment of the $H_2$ mole flow in the gas, whose specific heat is greater compared to the other components; (ii) the increase of the $N_2$ mole flow, in those cases of SNG + $N_2$ injection; and (iii) the decrease of the coke mass flow, in those cases of coke replacement. In (i) and (ii), cooling the gases requires to remove more energy, while in (iii), heating the solids requires less energy, what in both cases translates into an excess of available energy. In any case, if we consider the limitation imposed by the flame temperature on the maximum PtG capacity (see section 4.2.7), the $H_2$ utilization will not be greater than 0.7 for any configuration, which is still reasonable and according to literature (Nogami et al., 2012).

#### 4.2.5. $KPI_{07}$: percentage of direct reduction in the blast furnace

The direct reduction is and endothermic process that takes place in the lower part of the blast furnace. Since the injection of $H_2$ and SNG will provide less thermal energy than the fossil fuel they replace, the percentage of direct reduction will decrease to satisfy the energy balance (i.e., we have less endothermic reduction to compensate for the lack of thermal energy). In general, a higher decrease in direct reduction is

obtained for coke replacement compared to coal replacement, and for OBF in comparison to BF. Combining both trends, we observe that the decrease in the percentage of direct reduction is 40%–47% higher for OBF with coke replacement than for air-blown BF with coal replacement. Regarding the type of PtG used, the decrease is more pronounce for $H_2$ injections (6.3–8.8 pp/$\frac{MW_{PtG}}{t_{HM}/h}$) than for SNG injections (3.8–7.5 pp/$\frac{MW_{PtG}}{t_{HM}/h}$), because the former does not follow combustion when injected (remains as $H_2$), while methane follows partial combustion to CO and $H_2$ (i.e., provides more heat). The values for each case study can be seen in Table 3, and the graphical representation against $KPI_{01}$ in the appendix (see supplementary material). It should be noted that, in practice, the percentage of direct reduction should not fall below 5% (technical limitation according to (Babich, 2021)), what implies upper limits in the electrolysis capacity that can be integrated with OBF. These values are presented in Table 4, although they are less restrictive than the limitation imposed by the flame temperature (see section 4.2.7).

#### 4.2.6. $KPI_{08}$: recirculation ratio in OBF concepts

The recirculation ratio is defined as the percentage of BFG that is diverted to the carbon capture stage on account of the top gas recycling. This ratio is adjusted to always inject the same mole flow of $H_2$+CO as in the base case (18.5 kmol/$t_{HM}$), regardless of the BFG composition. Results show that the recirculation ratio decreases between 3 and 6 percentage points per $\frac{MW_{PtG}}{t_{HM}/h}$ of electrolysis capacity installed. In general, this decrease is about 50% higher in the case of coke replacement than in coal replacement. Comparing the different types of PtSNG, the decrease is greater the higher the amount of $H_2$ introduced in the methanation process per MW of electrolysis.

It should be mention that an increasing $\eta_{H_2}$ with the PtG capacity only means that the $H_2O$ mole flow in the BFG increases faster than the $H_2$ mole flow. The $H_2$ mole flow in the BFG increases because we are injecting $H_2$ or SNG in the blast furnace, whose H:C ratios are higher than those of coal and coke. In practice, this makes the required recirculation lower.

**Table 3**
Summary of the comparison of the 16 PtG integration cases (see Fig. 2 for simplified process flow diagrams).

| Type of PtG | $H_2$ | $H_2$ | $H_2$ | $H_2$ | SNG | SNG | SNG | SNG | SNG (+$N_2$) | SNG (+$N_2$) | SNG | SNG | SNG (+$N_2$) | SNG (+$N_2$) | SNG | SNG |
|---|---|---|---|---|---|---|---|---|---|---|---|---|---|---|---|---|
| $CO_2$ source for methanation | – | – | – | – | $CO_2$ | $CO_2$ | $CO_2$ | $CO_2$ | treated BFG | treated BFG | treated BFG | treated BFG | BFG | BFG | BFG | BFG |
| Type of BF | BF | BF | OBF | OBF | BF | BF | OBF | OBF | BF | BF | OBF | OBF | BF | BF | OBF | OBF |
| Fossil fuel replaced | coal | coke | coal | coke | coal | coke | coal | coke | coal | coke | coal | coke | coal | coke | coal | coke |
| Gas production $\left(\frac{kg}{h}/MW_{PtG}\right)$ | 20.0 | 20.0 | 20.0 | 20.0 | 41.0 | 41.0 | 41.0 | 41.0 | 230 | 213 | 64.2 | 58.5 | 155 | 154 | 52.7 | 52.5 |
| Fossil fuel replacement ratio $(kg_{fossil\ fuel}/kg_{gas})$ | 2.90 | 2.46 | 3.65 | 3.07 | 1.30 | 1.10 | 1.40 | 1.17 | 0.31 | 0.29 | 1.35 | 1.14 | 0.44 | 0.37 | 1.37 | 1.15 |
| $O_2$ saved in the ASU $\left(\frac{kg}{h}/MW_{PtG}\right)$ | 167 | 166 | 197 | 193 | 158 | 157 | 157 | 152 | 158 | 157 | 157 | 152 | 158 | 157 | 157 | 152 |
| Change in the gas utilization $\eta_{CO,H_2}$ $\left(pp/\frac{MW_{PtG}}{t_{HM}/h}\right)$ | −2.0 | −2.4 | +0.4 | −0.0 | −1.3 | −1.7 | −0.1 | −0.4 | −1.7 | −2.3 | −0.1 | −0.5 | −1.6 | −2.1 | −0.1 | −0.5 |
| Decrease in direct reduction $\left(pp/\frac{MW_{PtG}}{t_{HM}/h}\right)$ | 6.3 | 8.0 | 7.1 | 8.8 | 3.8 | 3.8 | 4.1 | 5.5 | 5.1 | 7.1 | 6.3 | 7.5 | 4.7 | 6.7 | 5.3 | 6.9 |
| Decrease in recirculation for TGR $\left(pp/\frac{MW_{PtG}}{t_{HM}/h}\right)$ | – | – | 3.64 | 5.54 | – | – | 3.07 | 4.64 | – | – | 4.57 | 6.05 | – | – | 3.85 | 5.69 |
| Decrease in $T_{flame}$ $\left(^{\circ}C/\frac{MW_{PtG}}{t_{HM}/h}\right)$ | 83.0 | 153 | 112 | 209 | 86.7 | 149 | 90.6 | 169 | 191 | 270 | 140 | 226 | 162 | 236 | 117 | 211 |
| Decrease in total $CO_2$ emissions $\left(\frac{kg}{h}/MW_{PtG}\right)$ | 163 | 160 | 204 | 199 | 150 | 147 | 161 | 157 | 203 | 197 | 248 | 215 | 188 | 186 | 204 | 199 |
| Change in the percentage of $CO_2$ that is emitted as pure $CO_2$ $\left(pp/\frac{MW_{PtG}}{t_{HM}/h}\right)$ | – | – | −3.6 | −12 | – | – | −13 | −19 | – | – | +12 | −4.8 | – | – | −0.2 | −8.9 |
| Net energy penalty $(MJ/kg_{CO2})$ | 18.3 | 19.2 | 13.5 | 14.5 | 19.6 | 20.6 | 17.8 | 18.9 | 12.9 | 14.0 | 10.1 | 11.9 | 14.7 | 15.4 | 12.6 | 13.6 |
| External power to satisfy electricity demand when the plant is no longer self-sufficient, per additional MW of PtG installed $(MW/MW_{PtG})$ | 0.94 | 0.91 | 0.96 | 0.91 | 0.94 | 0.91 | 0.93 | 0.91 | 0.98 | 0.93 | 1.02 | 0.93 | 0.95 | 0.91 | 0.95 | 0.91 |

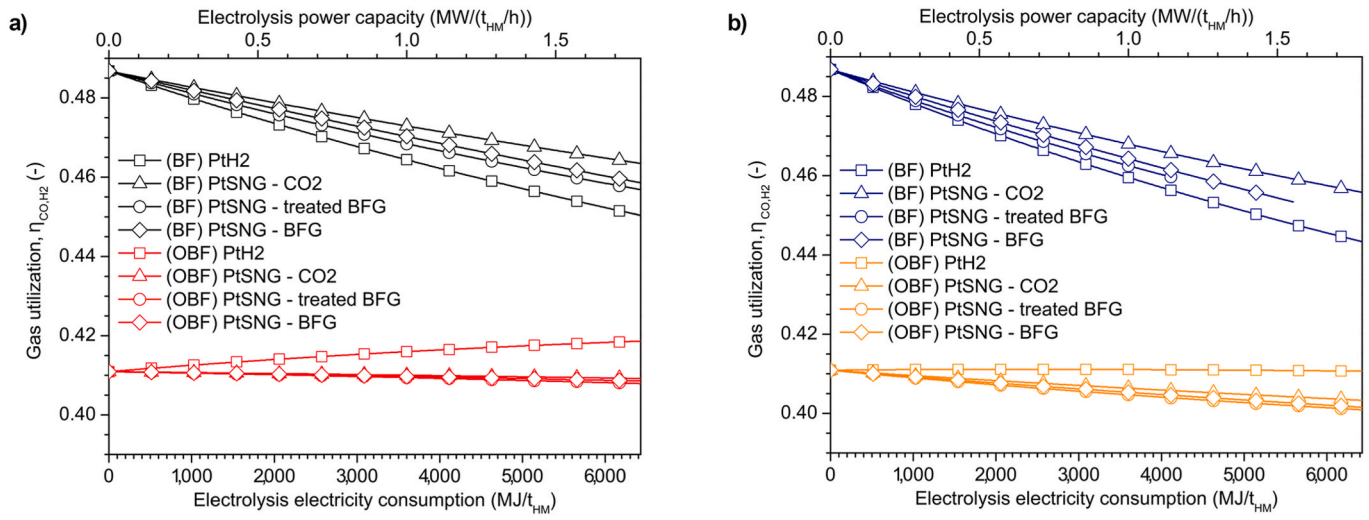


**Fig. 6.** Gas utilization, $\eta_{CO,H_2}$ (−) vs. Electrolysis electricity consumption (MJ/$t_{HM}$), in the case of a) coal replacement and b) coke replacement.

#### 4.2.7. $KPI_{09}$: flame temperature

The flame temperature decreases when injecting $H_2$, SNG or SNG + $N_2$ because of the lower thermal energy provided in comparison with the replaced fossil fuels (coal and coke). In terms of the installed electrolysis capacity, we found that the injection of $H_2$ may reduce the flame temperature by 83–209 °C, the injection of SNG by 87–226 °C, and the injection of SNG + $N_2$ by 162–270 °C, all of them per $\frac{MW_{PtG}}{t_{HM}/h}$. These wide ranges of values, which comprise the different types of configurations (BF/OBF, coal/coke replacement), come from the fact that each case produces a different amount of gas. When converting the results to °C drops per kg of gas injected, we found that the SNG cools the flame temperature by 2.2 °C per $kg_{SNG}/t_{HM}$ in coal replacements (in agreement with literature, 3.0 °C per $kg_{SNG}/t_{HM}$ (Bailera et al., 2021b)) and by 3.6–4.1 °C per $kg_{SNG}/t_{HM}$ in coke replacements (also in agreement with literature, 4.5 °C per $kg_{SNG}/t_{HM}$ (Babich et al., 2008)). Regarding $H_2$, it drops the flame temperature by 4.1–5.6 °C per $kg_{H2}/t_{HM}$ in coal replacements and by 7.6–10.4 °C per $kg_{H2}/t_{HM}$ in coke replacements.

In general, we see that the drop in the flame temperature is 61–87% higher for the coke replacement cases, in comparison to the coal replacement cases at the same electrolysis capacity. This is because the injection of coal itself already produces a reduction in the flame temperature. Therefore, by replacing it we avoid the temperature drop corresponding to the replaced amount of coal. Comparing our results for coke and coal replacements, we can deduce that the injection of coal results in a reduction of about 1.3 °C per $kg_{coal}/t_{HM}$. This is in agreement with the value provided by Babich for bituminous coals, which is 1.0–1.6 °C per $kg_{coal}/t_{HM}$ (bituminous coals have 60–80% of C content; the coal used in our model has 77%) (Babich, 2021).

The flame temperature is one of the most limiting factors when integrating Power to Gas. According to Babich (2021), some blast furnaces have been successfully operated with 1,600–1,700 °C flame temperatures (the lower the percentage of direct reduction, the lower the minimum limit for the flame temperature can be). Nevertheless, a minimum of 2,000 °C is generally considered in literature as a reasonable technical limit (Geerdes et al., 2020). According to the latter, the maximum electrolysis capacity that can be installed when replacing coke is 0.44–0.57 MW for SNG + $N_2$ injections, and 0.54–0.88 MW for SNG or $H_2$ injections, per $t_{HM}$/h produced in the blast furnace. When replacing coal, these upper limits increase to 0.61–0.86 MW for SNG + $N_2$ injections, and to 0.98–1.67 MW for SNG or $H_2$ injections, per $t_{HM}$/h produced in the blast furnace. In general, the limitation in the electrolysis capacity is more restrictive for OBF concepts than for BF (Fig. 7).

#### 4.2.8. $KPI_{10}$, $KPI_{11}$, $KPI_{12}$ and $KPI_{13}$: $CO_2$ emissions

Four KPIs were defined to characterize the $CO_2$ emissions: the total equivalent $CO_2$ emissions, the $CO_2$ emitted as pure $CO_2$ (i.e., that can be stored), the avoided $CO_2$ and the $CO_2$ in closed loop. The $CO_2$ emitted (total and captured) is presented in Fig. 8 (empty symbols for the total $CO_2$, and filled symbols for the captured $CO_2$). In general, the type of fossil fuel replaced has not a relevant influence on the total $CO_2$ emitted, and the OBF cases present faster decrease in the total $CO_2$ emissions. For most cases, the decrease in total $CO_2$ emissions is around the range

**Table 4**
Maximum PtG capacity that can be installed according to different limiting factors, for the 16 PtG integration cases. The units are MW of electrolysis per $t_{HM}$/h produced in the blast furnace.

| Type of PtG | $H_2$ | $H_2$ | $H_2$ | $H_2$ | SNG | SNG | SNG | SNG | SNG (+$N_2$) | SNG (+$N_2$) | SNG | SNG | SNG (+$N_2$) | SNG (+$N_2$) | SNG | SNG |
|---|---|---|---|---|---|---|---|---|---|---|---|---|---|---|---|---|
| $CO_2$ source for methanation | – | – | – | – | $CO_2$ | $CO_2$ | $CO_2$ | $CO_2$ | treated BFG | treated BFG | treated BFG | treated BFG | BFG | BFG | BFG | BFG |
| Type of BF | BF | BF | OBF | OBF | BF | BF | OBF | OBF | BF | BF | OBF | OBF | BF | BF | OBF | OBF |
| Fossil fuel replaced | coal | coke | coal | coke | coal | coke | coal | coke | coal | coke | coal | coke | coal | coke | coal | coke |
| Limited by ≥ 5% direct reduction | – | – | 1.53 | 1.23 | – | – | 2.65 | 1.98 | – | – | 1.72 | 1.45 | – | – | 2.05 | 1.57 |
| Limited by ≥ 2000 °C flame temperature | 1.67 | 0.87 | 1.22 | 0.62 | 1.59 | 0.88 | 1.50 | 0.77 | 0.61 | 0.44 | 0.98 | 0.54 | 0.86 | 0.57 | 1.18 | 0.62 |
| Limited by electricity self-sufficiency | 0.29 | 0.30 | 0.07 | 0.08 | 0.29 | 0.30 | 0.07 | 0.08 | 0.27 | 0.28 | 0.07 | 0.07 | 0.29 | 0.30 | 0.07 | 0.08 |

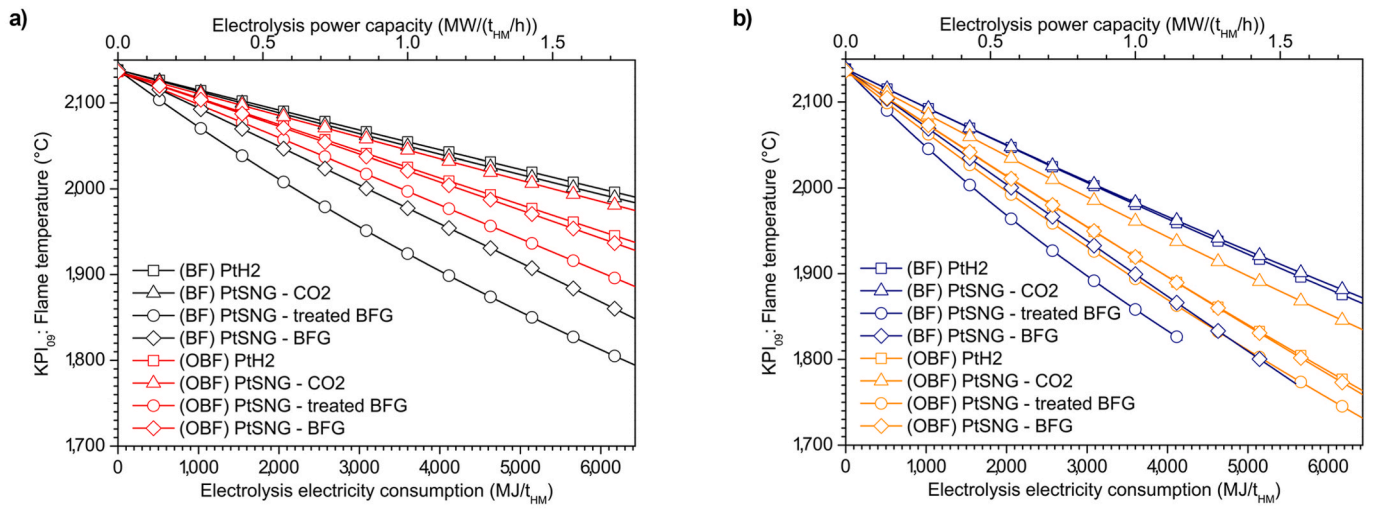


**Fig. 7.** Flame temperature (°C) vs. Electrolysis electricity consumption (MJ/$t_{HM}$), in the case of a) coal replacement and b) coke replacement.

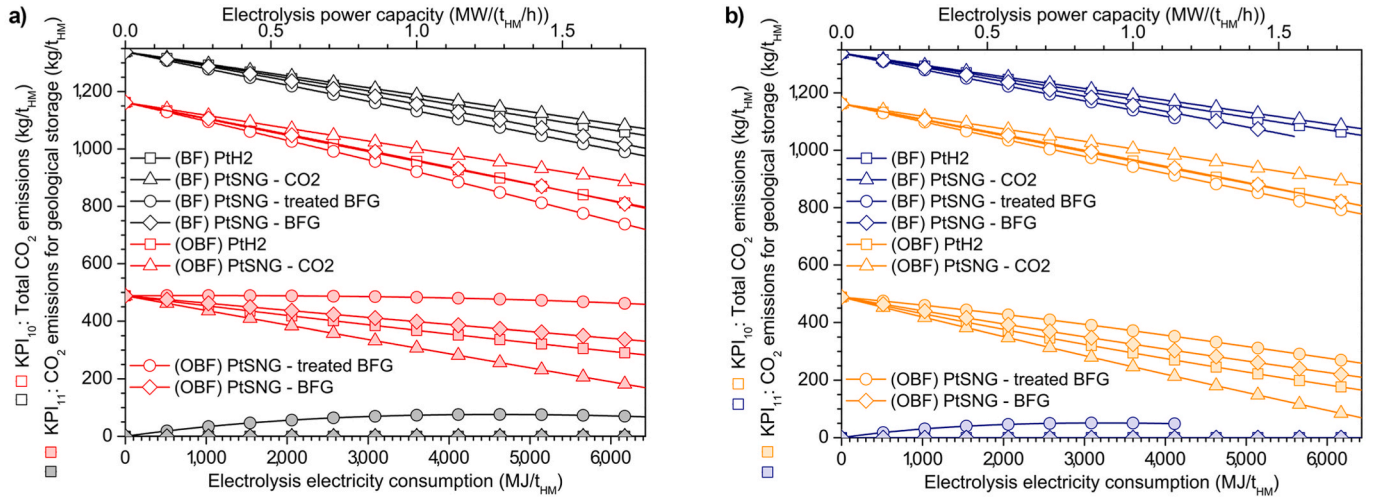


**Fig. 8.** Total $CO_2$ emissions (kg/tHM) and $CO_2$ emissions that can be stored in geological reservoirs (kg/$t_{HM}$) vs. Electrolysis electricity consumption (MJ/$t_{HM}$), in the case of a) coal replacement and b) coke replacement.

150–215 $kg_{CO2}$/h per MW of electrolysis. The most limited configuration is the PtG integration that uses pure $CO_2$ in the methanation, whose maximum $CO_2$ cut rate is 160 $kg_{CO2}$/h per MW of electrolysis. The percentage of the cut $CO_2$ that is kept in closed loop thanks to methanation is 72%–74% for BF configurations and 67%–69% for OBF. The rest of the contribution to the decrease in $CO_2$ emissions mainly comes from the increment of the H:C ratio in the reducing agents.

Regarding the $CO_2$ available for storage, this is a parameter useful mainly for the OBF cases, since they include the amine carbon capture plant. It can be seen that the mass flow of $CO_2$ that is emitted as pure $CO_2$ decreases with the electrolysis capacity installed. This is because the captured $CO_2$ is consumed in methanation and/or because the recirculation ratio decreases (i.e., decreases the amount of BFG passing through the amine scrubbing). Nevertheless, in the case of using treated BFG for methanation (for coal replacement), the drop in the available pure $CO_2$ is slower than the decrease in total $CO_2$ emissions, so the relative percentage increases. For this reason, this configuration is recommended against the others. The variation in the percentage of $CO_2$ emitted as pure $CO_2$, with respect to the total $CO_2$ emissions, is included in Table 3 (in the base case, 42% of the total emissions comes from the amine plant as captured $CO_2$). It is worth to note that, in the case of air-blown BF integrations, there will be $CO_2$ coming from the amine scrubbing when the methanation consumes treated BFG, although not in a significant amount.

#### 4.2.9. $KPI_{14}$ and $KPI_{15}$: gross and net energy penalty

The gross and net energy penalty were defined in terms of electricity consumption according to Eq. (20) and Eq. (21). In general, the energy penalty barely changes with the size of the PtG plant. It can decrease to some extent due to the change in composition of the BFG entering the methanation (more $H_2$ available) or increase because of the $O_2$ that remains unused when the ASU is no longer needed. However, the energy penalty does changes significantly from one PtG integration to another. The highest net energy penalty (20.6 MJ/$kg_{CO2}$) is twice the amount of the lowest net energy penalty (10.1 MJ/$kg_{CO2}$). The former corresponds to the case of BF integrated with PtSNG using pure $CO_2$ for coke replacement, while the latter to an OBF integrated with PtSNG using treated BFG for coal replacement. Therefore, selecting the proper type of integration is crucial when applying Power to Gas to ironmaking.

#### 4.2.10. $KPI_{16}$ and $KPI_{17}$: electricity and thermal self-sufficiency

To keep self-sufficiency is key when aiming to modify an existing ironmaking plant. In the case of PtG integrations, this is a strong limitation because of the large consumption of the electrolyzer. In the case of

BF, the largest PtG capacity to remain self-sufficient is around 0.30 MW per $t_{HM}$/h. This corresponds to the 18%–64% of the maximum limit established by the flame temperature criterion. The situation is even worse for the case of OBF, whose limit of self-sufficiency is at 0.08 MW per $t_{HM}$/h because a large amount of BFG is used for top gas recycling instead for power production. This corresponds just to the 5%–13% of the capacity that could be installed without decreasing the flame temperature below 2,000 °C (Table 4). Thus, if significant $CO_2$ reductions are aimed through PtG, it should be expected that self-sufficiency in electricity will not be achieved. At least, for each additional MW of PtG above the self-sufficiency limit, we only need to consume 0.91–0.98 MW of external power thanks to the increment in the available thermal energy from the gases produced in the ironmaking plant.

### 4.3. Comparing the limits of the different integrations of power to gas in ironmaking

As we have seen, the maximum PtG capacity to install in blast furnace ironmaking may be limited by the percentage of direct reduction (≥5%), the flame temperature (≥2,000 °C) and the electricity self-sufficiency (Table 4). In most cases, the former can be ignored because it allows installing twice the capacity compared to the other limiting factors. Only if we were to consider flame temperatures below 2,000 °C (justified by the low direct reduction share (Babich, 2021)), it might become a relevant limitation for the case of $PtH_2$ in OBF with coal replacement. Regarding self-sufficiency, it imposes an excessive limitation in the PtG to install, which leads to $CO_2$ cuts that are not worth the effort. Less than 4.5% of the total $CO_2$ emitted would be avoided in BF integrations, and less than 1.7% in OBF. Nevertheless, the self-sufficiency limitation could be used as a benchmark for large pilot plants to improve their know-how without jeopardizing the operational reliability of the ironmaking plant. For example, in blast furnaces of 500 $t_{HM}$/h size (Bailera et al., 2021a), the maximum electrolysis capacity for these large scale research projects would be 150 MW in the case of BF and 35 MW for OBF, which is in the range of the current state-of-the-art of the electrolysis technology (Schröcker et al., 2021). These examples, based on the typical size of a commercial BF (500 $t_{HM}$/h), are given as an illustration to estimate the PtG capacity that would be required in a real case, instead of only providing the specific value that is dependent on the hot metal production. The objective is to give clearer conclusions to the reader, which is assumed to be more familiar with the MW units rather than with the MW/($t_{HM}$/h) units.

Thus, the limitation imposed by the flame temperature will be used as the standard of comparison for the different PtG integrations. In Fig. 9, the most relevant KPIs are normalized and compared for the 16 case studies. The maximum PtG to install and the power required from an external power plant are normalized with respect to 1.67 $MW_{PtG}/\frac{t_{HM}}{h}$ (i.e., the global maximum of the installable PtG), the total $CO_2$ emissions and those from amine scrubbing are normalized with respect to 1,338 $kg/t_{HM}$ (i.e., the $CO_2$ emissions of the BF base case), and the energy penalty is normalized with respect to 20.6 $MJ/kg_{CO2}$ (i.e., the global maximum). It can be seen that the PtSNG integration consuming treated BFG, when applied to OBF, has the lowest energy penalty and the highest percentage of $CO_2$ available as pure $CO_2$ among all case studies. Moreover, it is one of the lowest $CO_2$ emitters, while requiring the lowest PtG capacity of all the OBF concepts. Therefore, this configuration should be preferred over any other. If we stick to the BF concepts (since OBF are not yet commercial), it will depend on how ambitious the target for total $CO_2$ emission reduction is. For 10% $CO_2$ reductions, the PtSNG integration using treated BFG is still the best configuration, but if we aim for 20% $CO_2$ reductions, $PtH_2$ might be the right solution (its figures are similar to those of PtSNG using pure $CO_2$, but the latter would involve higher cost due to the additional equipment).

## 5. Conclusions

In this article we analyzed and compared 16 Power to Gas integrations for blast furnace ironmaking, by using 17 key performance indicators. The integrations included 4 types of PtG ($PtH_2$, PtSNG using pure $CO_2$, PtSNG using treated BFG, and PtSNG using BFG), two types of blast furnaces (air-blown and oxygen) and two types of fossil replacement (coal or coke). The KPI covered technical, energy and environmental aspects of the process. For the modelling of the blast furnaces we used the Rist diagram, validated with literature data (<2% deviation).

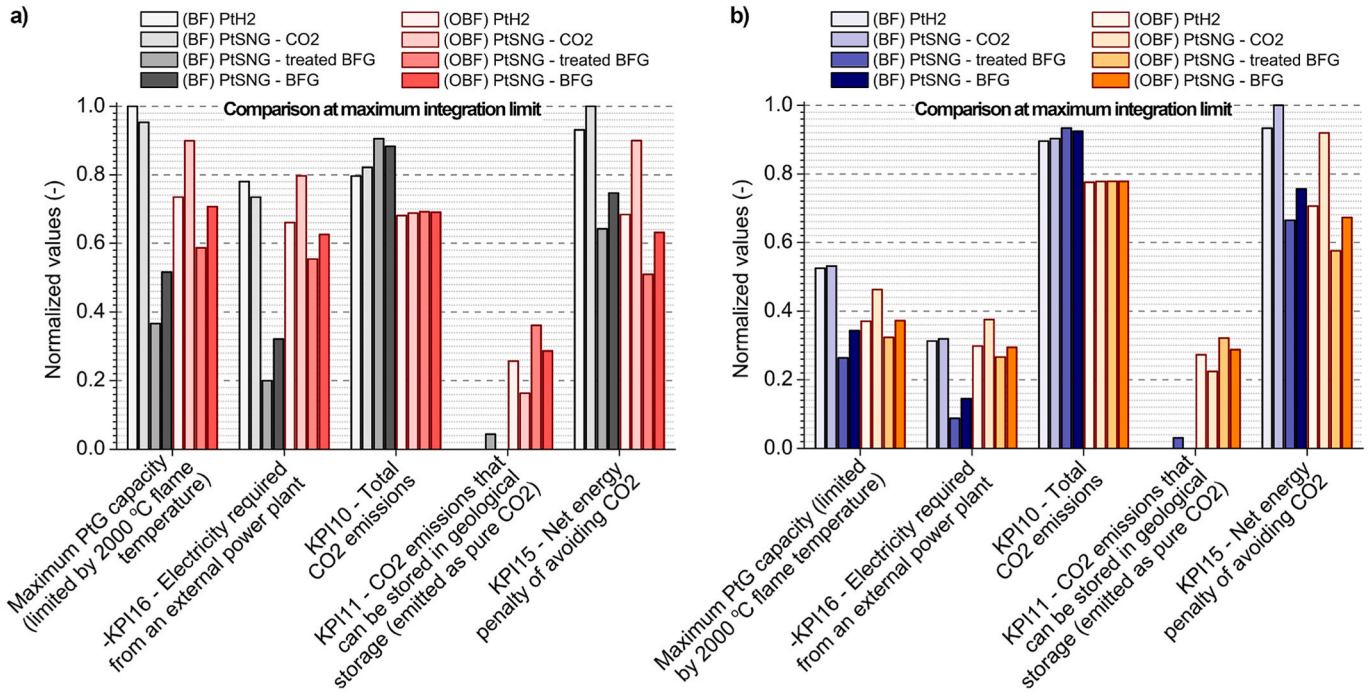


**Fig. 9.** Comparison of $KPI_{16}$, $KPI_{10}$, $KPI_{11}$ and $KPI_{15}$ at the maximum PtG capacity that can be installed in each configuration (limited by the decrease of the flame temperature) in the case of a) coal replacement and b) coke replacement. The values are normalized for readability.

The results of the study were provided as a function of the PtG capacity installed per $t_{HM}$/h produced in the blast furnace, in order to make them scalable to any size of PtG and ironmaking plant.

Regarding technical aspects, results show that integrating PtG decreases moderately the utilization of the reducing gas (up to 2.4 percentage points per MW/($t_{HM}$/h)). The percentage of direct reduction also diminish, by 6.3–8.8 percentage points per MW/($t_{HM}$/h) for $H_2$ injections, and by 3.8–7.5 percentage points per MW/($t_{HM}$/h) for SNG injections. The fossil fuel replacement ratios were found to be in agreement with literature. In the case of coke, these are 1.10–1.15 for SNG, and 2.46–3.07 for $H_2$ (when coke was replaced, coal was kept constant at 200 kg/$t_{HM}$). In the case of coal replacement, the values are 1.30–1.40 for SNG, and 2.90–3.65 for $H_2$ (when coal was replaced, coke was kept constant at 289.0 and 234.8 kg/$t_{HM}$, for BF and OBF respectively). In addition, the SNG cools the flame temperature by 2.2 °C per $kg_{SNG}/t_{HM}$ in coal replacements and by 3.6–4.1 °C per $kg_{SNG}/t_{HM}$ in coke replacements. The $H_2$ injection drops the flame temperature by 4.1–5.6 °C per $kg_{H2}/t_{HM}$ in coal replacements and by 7.6–10.4 °C per $kg_{H2}/t_{HM}$ in coke replacements.

Regarding energy and environmental aspects, results show that PtG integrations may avoid the ASU, thanks to the $O_2$ by-produced in the electrolysis, when the PtG capacity is above 0.57–0.61 MW/($t_{HM}$/h) in BF, and above 1.71–2.19 MW/($t_{HM}$/h) in OBF. For most cases, the decrease in total $CO_2$ emissions is around 150–215 $kg_{CO2}/t_{HM}$ per MW/($t_{HM}$/h). The most limited configuration is the PtG integration that uses pure $CO_2$ in the methanation, whose maximum $CO_2$ cut rate is 160 $kg_{CO2}/t_{HM}$ per MW/($t_{HM}$/h). The energy penalty (in terms of electricity consumption) was found to be mostly independent on the size of the PtG plant, but greatly dependent on the type of integration. The highest net energy penalty was 20.6 MJ/$kg_{CO2}$ (BF integrated with PtSNG using pure $CO_2$ for coke replacement), while the lowest was 10.1 MJ/$kg_{CO2}$ (OBF integrated with PtSNG using treated BFG for coal replacement).

In practice, the maximum PtG capacity to install is limited by the decrease in the flame temperature (from 0.5 to 1.7 MW/($t_{HM}$/h) depending on the integration) and by the requirement of remaining self-sufficient in electricity consumption (<0.30 MW/($t_{HM}$/h) in BF, and <0.08 MW/($t_{HM}$/h) in OBF). The latter imposes an excessive limitation in the PtG to install, making the $CO_2$ cuts not worth the effort (<4.5% in BF, and <1.7% in OBF). The self-sufficiency limitation should be understood as a benchmark for PtG research projects aiming for operating pilot plants without jeopardizing the operational reliability of the ironmaking plant. For example, in blast furnaces of 500 $t_{HM}$/h size (Bailera et al., 2021a), the maximum electrolysis capacity for these large scale research projects would be 150 MW in the case of BF and 35 MW for OBF, which is in the range of the current state-of-the-art of the electrolysis technology.

If significant $CO_2$ reductions are aimed through PtG, it should be taken the limitation related to the flame temperature as standard (which is less restrictive), having in mind that the ironmaking plant will be no longer self-sufficient in electricity (in this case, the electricity purchased from the grid should come from renewable energy sources to not produce additional $CO_2$ emissions). Among all case studies, the lowest energy penalty is found for the OBF-PtSNG integration that consumes treated BFG and replaces coal. This configuration has one of the highest reduction in $CO_2$ emissions, even though it requires the lowest PtG capacity in comparison with the other OBF concepts. Furthermore, it provides the highest percentage of $CO_2$ emitted as pure $CO_2$ (i.e., more $CO_2$ can be diverted directly to storage). Therefore, this configuration should be preferred against any other. As an example, if we assume a 500 $t_{HM}$/h blast furnace (typical commercial BF) to estimate the total PtG capacity in a real steel plant, the PtG capacity of this concept could be as large as 490 MW, and could avoid up to 21% of the $CO_2$ emissions. If we stick to the BF concepts (since OBF are not yet commercial), the selection of the best type of integration will depend on how ambitious the target for total $CO_2$ emission reduction is. For 10% $CO_2$ reductions, the PtSNG integration using treated BFG is still the best configuration, but if we aim for 20% $CO_2$ reductions, $PtH_2$ might be the right solution (up to 835 MW of $PtH_2$ to avoid 20.3% of the $CO_2$ emissions, if coal is replaced).

## CRediT authorship contribution statement

**Manuel Bailera:** Conceptualization, Methodology, Software, Validation, Formal analysis, Investigation, Resources, Writing – original draft, Visualization, Supervision, Funding acquisition. **Takao Nakagaki:** Conceptualization, Validation, Resources, Writing – original draft, Supervision. **Ryoma Kataoka:** Software, Validation, All authors have read and agreed to the published version of the manuscript.

## Declaration of competing interest

The authors declare that they have no known competing financial interests or personal relationships that could have appeared to influence the work reported in this paper.

## Data availability

No data was used for the research described in the article.

## Acknowledgments

This project has received funding from the European Union's Framework Programme for Research and Innovation Horizon 2020 (2014–2020) under the Marie Skłodowska-Curie Grant Agreement No. 887077.

## Appendix A. Supplementary data

Supplementary data to this article can be found online at https://doi.org/10.1016/j.jclepro.2022.134038.

## Nomenclature

*Acronyms*

| | |
|---|---|
| ASU | air separation unit |
| BF | blast furnace (air-blown, unless otherwise specified) |
| BFG | blast furnace gas |
| COG | coke oven gas |
| HM | hot metal |
| KPI | key performance indicator |
| LHV | lower heating value |
| OBF | oxygen blast furnace |

| | |
|---|---|
| PFD | process flow diagram |
| pp | percentage points |
| PtG | Power to Gas |
| $PtH_2$ | Power to Hydrogen |
| PtSNG | Power to Synthetic natural gas |
| TGR | top gas recycling |

*Symbols*

| | |
|---|---|
| $a_j$ | number of moles of $H_2$ in injectant j per number of moles of injectant j, $mol_{H2}/mol_j$ |
| $b_j$ | number of moles of $O_2$ in injectant j per number of moles of injectant j, $mol_{O2}/mol_j$ |
| $G_i$ | Gibbs free energy of reaction *i*, J/mol |
| $g_i$ | Gibbs free energy of component *i*, J/mol |
| $h_i$ | enthalpy of component *i*, J/mol |
| $Kp_i$ | equilibrium constant of reaction *i*, |
| $m$ | mass flow, $kg/t_{HM}$ |
| $P$ | pressure, bar |
| $Q$ | thermal energy, $MJ/t_{HM}$ |
| $R$ | ideal gas constant, J/(mol·K) |
| rr | replacement ratio, |
| $s_i$ | entropy of component *i*, J/(mol·K) |
| $T$ | temperature, K |
| $W$ | electrical consumption, $MJ/t_{HM}$ |
| X | abscissa in the Rist diagram, $(mol_O + mol_{H2})/(mol_C + mol_{H2})$ |
| $x_d$ | number of moles of O removed from wüstite by direct reduction per total moles of reducing gas mixture, $mol_O/(mol_C + mol_{H2})$ |
| $x_e$ | number of moles of $H_2O$ in hot blast per total moles of reducing gas mixture, $mol_{H2O}/(mol_C + mol_{H2})$ |
| $x_i$ | number of moles of O transferred from the iron oxides to the gas by indirect reduction per total moles of reducing gas mixture, $mol_O/(mol_C + mol_{H2})$ |
| $x_j$ | number of moles of injectant j (overall formula $CH_{2a}O_{2b}N_{2c}S_{2d}Z_z$, $H_{2a}O_{2b}N_{2c}$ or $O_{2b}N_{2c}$) per total moles of reducing gas mixture, $mol_j/(mol_C + mol_{H2})$ |
| $x_k$ | number of moles of $H_2$ in the coke per total moles of reducing gas mixture, $mol_{H2}/(mol_C + mol_{H2})$ |
| $x_{Mn}$ | number of moles of O removed by direct reduction of MnO per total moles of reducing gas mixture, $mol_O/(mol_C + mol_{H2})$ |
| $x_P$ | number of moles of O removed by direct reduction of $P_2O_5$ per total moles of reducing gas mixture, $mol_O/(mol_C + mol_{H2})$ |
| $x_S$ | number of moles of O replaced by S in the slag per total moles of reducing gas mixture, $mol_O/(mol_C + mol_{H2})$ |
| $x_{Si}$ | number of moles of O removed by direct reduction of $SiO_2$ per total moles of reducing gas mixture, $mol_O/(mol_C + mol_{H2})$ |
| $x_v$ | number of moles of O in hot blast per total moles of reducing gas mixture, $mol_O/(mol_C + mol_{H2})$ |
| Y | ordinate in the Rist diagram, $(mol_O + mol_{H2})/mol_{Fe}$ |
| $y_d$ | number of moles of O removed from wüstite by direct reduction per mol of Fe produced, $mol_O/mol_{Fe}$ |
| $y_e$ | number of moles of $H_2O$ in hot blast per mol of Fe produced, $mol_{H2O}/mol_{Fe}$ |
| $Y_E$ | intercept of the operating line representing the moles of $H_2$ and O coming from sources other than iron oxides that contribute to the formation of the reducing gas per mol of Fe produced (negative sign by convention), $(mol_O + mol_{H2})/mol_{Fe}$ |
| $y_i$ | number of moles of O transferred from the iron oxides to the gas by indirect reduction per mol of Fe produced, $mol_O/mol_{Fe}$ |
| $y_j$ | number of moles of injectant j (overall formula $CH_{2a}O_{2b}N_{2c}S_{2d}Z_z$, $H_{2a}O_{2b}N_{2c}$ or $O_{2b}N_{2c}$) per mol of Fe produced, $mol_j/mol_{Fe}$ |
| $y_k$ | number of moles of $H_2$ in the coke per mol of Fe produced, $mol_{H2}/mol_{Fe}$ |
| $y_{Mn}$ | number of moles of O removed by direct reduction of MnO per mol of Fe produced, $mol_O/mol_{Fe}$ |
| $y_P$ | number of moles of O removed by direct reduction of $P_2O_5$ per mol of Fe produced, $mol_O/mol_{Fe}$ |
| $y_S$ | number of moles of O replaced by S in the slag per mol of Fe produced, $mol_O/mol_{Fe}$ |
| $y_{Si}$ | number of moles of O removed by direct reduction of $SiO_2$ per mol of Fe produced, $mol_O/mol_{Fe}$ |
| $y_v$ | number of moles of O in hot blast per mol of Fe produced, $mol_O/mol_{Fe}$ |

*Greek symbols*

| | |
|---|---|
| μ | slope of the Rist diagram, i.e., number of moles of reducing gas per mol of Fe produced, $(mol_C + mol_{H2})/mol_{Fe}$ |
| $\mu_i$ | mole production of product *i* (Stoichiometric coefficient), kmol |
| $\eta_{CO}$ | CO utilization factor, defined as the quotient $CO_2/(CO + CO_2)$ of the molar fractions in the BFG, |
| $\eta_{CO,H_2}$ | reducing gas utilization factor, defined as the quotient $(CO_2+H_2O)/(CO + CO_2+H_2+H_2O)$ of the molar fractions in the BFG, |
| $\eta_{H2}$ | $H_2$ utilization factor, defined as the quotient $H_2O/(H_2+H_2O)$ of the molar fractions in the BFG, |
| $\eta_{pp}$ | power plant efficiency |
| $\nu_i$ | mole consumption of reagent *i* (Stoichiometric coefficient), kmol |
| $\omega_i$ | mass fraction of component *i* in coal, % (dry basis) |

*Subscripts and superscripts*

| | |
|---|---|
| A | initial oxidation state of the iron oxides at the inlet of the blast furnace |
| $a$ | ambient pressure |
| $a,m$ | related to amine scrubbing and methanation |
| $ASU,m$ | electricity saved in the ASU thanks to the PtG integration |
| $ex,m$ | related to the exothermal heat of methanation |

| | |
|---|---|
| $k$ | fossil fuel (coke or coal) |
| $P$ | characteristic point of the operating line referring to the energy balance of the blast furnace |
| $p,m$ | related to preheating and methanation |
| $R$ | characteristic point of the operating line referring to the thermal reserve zone |
| $r$ | reactor |

## References


n.d. ArcelorMittal. ArcelorMittal asturias (Gijón) [WWW Document]. URL. https://spain.arcelormittal.com/what-we-do/lce/gijon.aspx. accessed 12.1.2021.

n.d. ArcelorMittal. ArcelorMittal Gijón [WWW Document]. URL. https://barsandrods.arcelormittal.com/mills/verina. accessed 12.1.2021.

Babich, A., 2021. Blast furnace injection for minimizing the coke rate and CO2 emissions. Ironmak. Steelmak. 48, 728–741. https://doi.org/10.1080/03019233.2021.1900037.

Babich, A., Senk, D., Gudenau, H., Mavrommatis, K.T., 2008. Ironmaking Textbook. RWTH Aachen University.

Babich, A., Senk, D., Solar, J., de Marco, I., 2019. Efficiency of biomass use for blast furnace injection. ISIJ Int. 59, 2212–2219. https://doi.org/10.2355/isijinternational.ISIJINT-2019-337.

Bailera, M., Lisbona, P., Peña, B., Romeo, L.M., 2021a. A review on CO2 mitigation in the Iron and Steel industry through Power to X processes. J. CO2 Util. 46, 101456 https://doi.org/10.1016/j.jcou.2021.101456.

Bailera, M., Lisbona, P., Peña, B., Romeo, L.M., 2020. Energy Storage. Springer. Springer International Publishing, Cham. https://doi.org/10.1007/978-3-030-46527-8.

Bailera, M., Lisbona, P., Romeo, L.M., 2019. Avoidance of partial load operation at coal-fired power plants by storing nuclear power through power to gas. Int. J. Hydrogen Energy 44. https://doi.org/10.1016/j.ijhydene.2019.08.033.

Bailera, M., Nakagaki, T., Kataoka, R., 2021b. Revisiting the Rist diagram for predicting operating conditions in blast furnaces with multiple injections. Open Res. Eur. 1 https://doi.org/10.12688/openreseurope.14275.1.

Bargiacchi, E., Candelaresi, D., Valente, A., Spazzafumo, G., Frigo, S., 2021. Life cycle assessment of substitute natural gas production from biomass and electrolytic hydrogen. Int. J. Hydrogen Energy 46, 35974–35984. https://doi.org/10.1016/j.ijhydene.2021.01.033.

Brower, R.C., Toxopeus, H.L., 1991. Massive coal injection at Hoogovens IJmuiden blast furnaces. Rev. Métall. 88, 323–334. https://doi.org/10.1051/metal/199188040323.

Davies, J., Dolci, F., Weidner, E., 2021. Historical analysis of FCH 2 JU electrolyser projects. https://doi.org/10.2760/951902.

De Ras, K., Van de Vijver, R., Galvita, V.V., Marin, G.B., Van Geem, K.M., 2019. Carbon capture and utilization in the steel industry: challenges and opportunities for chemical engineering. Curr. Opin. Chem. Eng. 26, 81–87. https://doi.org/10.1016/j.coche.2019.09.001.

Fenton, M.D., Tuck, C.A., 2019. Iron and Steel. 2016 Minerals Yearbook. US Geological Survey.

Gao, J., Wang, Y., Ping, Y., Hu, D., Xu, G., Gu, F., Su, F., 2012. A thermodynamic analysis of methanation reactions of carbon oxides for the production of synthetic natural gas. RSC Adv. 2, 2358–2368. https://doi.org/10.1039/c2ra00632d.

Geerdes, M., Chaigneau, R., Lingiardi, O., Molenaar, R., van, O., R, S.Y., Warren, J., 2020. Modern Blast Furnace Ironmaking an Introduction. IOS Press.

Hisashige, S., Nakagaki, T., Yamamoto, T., 2019. CO2 emission reduction and exergy analysis of smart steelmaking system adaptive for flexible operating conditions. ISIJ Int. 59, 598–606. https://doi.org/10.2355/isijinternational.ISIJINT-2018-355.

Holz, F., Scherwath, T., Valentin, I., Skar, C., Maranon-Ledesma, H., Crespo del Granado, P., Ramos, A., Olmos, L., Ploussard, Q., Lumbreras, S., Herbst, A., Fleiter, T., 2018. Case Study Report on the Role for Carbon Capture, Transport and Storage in Electricity and Industry in the Future.

International Energy Agency, 2020. Iron and Steel Technology Roadmap, Energy Technology Perspectives Series.

Izumiya, K., Shimada, I., 2021. Methane producing technology from CO2 for carbon recycling. In: The First Symposium on Carbon Ultimate Utilization Technologies for the Global Environment, CUUTE-1, pp. 34–35.

Jin, P., Jiang, Z., Bao, C., Lu, Y., Zhang, J., Zhang, X., 2016. Mathematical modeling of the energy consumption and carbon emission for the oxygen blast furnace with top gas recycling. Steel Res. Int. 87, 320–329. https://doi.org/10.1002/srin.201500054.

Kamijo, T., Noborisato, T., Morihiro, T., 2021. Advanced KM CDR ProcessTM and new KS-21 SolventTM. In: The First Symposium on Carbon Ultimate Utilization Technologies for the Global Environment, CUUTE-1, pp. 82–83.

Kim, Y.K., Lee, E.B., 2018. Optimization simulation, using steel plant off-gas for power generation: a life-cycle cost analysis approach. Energies 11. https://doi.org/10.3390/en11112884.

Lisbona, P., Bailera, M., Peña, B., Romeo, L.M., 2020. Integration of CO2 capture and conversion. In: Rahimpour, M.R., Farsi, M., Makarem, M.A. (Eds.), Advances in Carbon Capture. Woodhead Publishing, pp. 503–522. https://doi.org/10.1016/B978-0-12-819657-1.00022-0.

Meysson, N., Weber, J., Rist, A., 1964. Représentation graphique de la décomposition des carbonates dans le haut fourneau. Rev. Métall. 61, 623–633. https://doi.org/10.1051/metal/196461070623.

Nogami, H., Kashiwaya, Y., Yamada, D., 2012. Simulation of blast furnace operation with intensive hydrogen injection. ISIJ Int. 52, 1523–1527. https://doi.org/10.2355/isijinternational.52.1523.

Pandiello, Ó., 2019. El grupo 1 de la térmica de Aboño comenzará a funcionar con los gases siderúrgicos de Arcelor. ElComercio.

Perpiñán, J., Bailera, M., Romeo, L.M., Peña, B., Eveloy, V., 2021. CO2 recycling in the iron and steel industry via power to gas and oxy-fuel combustion. Energies 14, 7090. https://doi.org/10.3390/en14217090.

Quader, M.A., Ahmed, Shamsuddin, Ghazilla, R.A.R., Ahmed, Shameem, Dahari, M., 2015. A comprehensive review on energy efficient CO2 breakthrough technologies for sustainable green iron and steel manufacturing. Renew. Sustain. Energy Rev. 50, 594–614. https://doi.org/10.1016/j.rser.2015.05.026.

Rainer Remus, M.A.A.-M., Serge Roudier, L.D.S., 2013. Best available techniques (BAT) reference document for iron and steel production. https://doi.org/10.2791/98516.

Rist, A., Meysson, N., 1967. A dual graphic representation of the blast-furnace mass and heat balances. JOM (J. Occup. Med.) 19, 50–59. https://doi.org/10.1007/bf03378564.

Robles, B., Baeza, A., Mora, J.C., Corbacho, J.A., Trueba, C., Miralles, Y., 2014. Estudio del Impacto Radiológico de la Central Térmica de Carbón de Aboño.

Rosenfeld, D.C., Böhm, H., Lindorfer, J., Lehner, M., 2020. Scenario analysis of implementing a power-to-gas and biomass gasification system in an integrated steel plant: a techno-economic and environmental study. Renew. Energy 147, 1511–1524. https://doi.org/10.1016/j.renene.2019.09.053.

Sahu, R.K., Roy, S.K., Sen, P.K., 2015. Applicability of top gas recycle blast furnace with downstream integration and sequestration in an integrated steel plant. Steel Res. Int. 86, 502–516. https://doi.org/10.1002/srin.201400196.

Sato, M., Takahashi, K., Nouchi, T., Ariyama, T., 2015. Predictcion of next-generation ironmaking process based on oxygen blast furnace suitable for CO2 mitigation and energy flexibility. ISIJ Int. 55, 2105–2114. https://doi.org/10.2355/isijinternational.ISIJINT-2015-264.

Schröcker, D., Wille, A., Sentis, P., 2021. Pilot industrial technology prospect report: R&I evidence on EU development of low-carbon industrial technologies. https://doi.org/10.2777/48648.

Shao, L., Wang, Q., Qu, Y., Saxén, H., Zou, Z., 2021. A numerical study on the operation of the H2 shaft furnace with top gas recycling. Metall. Mater. Trans. B 52, 451–459. https://doi.org/10.1007/s11663-020-02020-6.

Suzuki, K., Hayashi, K., Kuribara, K., Nakagaki, T., Kasahara, S., 2015. Quantitative evaluation of CO2 emission reduction of active carbon recycling energy system for ironmaking by modeling with aspen plus. ISIJ Int. 55, 340–347. https://doi.org/10.2355/isijinternational.55.340.

Thema, M., Bauer, F., Sterner, M., 2019. Power-to-Gas: electrolysis and methanation status review. Renew. Sustain. Energy Rev. 112, 775–787. https://doi.org/10.1016/j.rser.2019.06.030.

Ueckerdt, F., Bauer, C., Dirnaichner, A., Everall, J., Sacchi, R., Luderer, G., 2021. Potential and risks of hydrogen-based e-fuels in climate change mitigation. Nat. Clim. Change 11, 384–393. https://doi.org/10.1038/s41558-021-01032-7.

Wu, J., Wang, R., Pu, G., Qi, H., 2016. Integrated assessment of exergy, energy and carbon dioxide emissions in an iron and steel industrial network. Appl. Energy 183, 430–444. https://doi.org/10.1016/j.apenergy.2016.08.192.